Mon. Not. R. Astron. Soc. **308**, 863–875 (1999)

Spinning test particles in a Kerr field – I

O. Semerák★

Department of Theoretical Physics, Faculty of Mathematics and Physics, Charles University, V Holešovičkách 2, CZ-180 00 Praha 8, Czech Republic

Accepted 1999 April 29. Received 1999 April 29; in original form 1997 May 2

ABSTRACT

Mathisson–Papapetrou equations are solved numerically to obtain trajectories of spinning test particles in (the meridional section of) the Kerr space–time. The supplementary conditions $p_\sigma S^{\mu\sigma} = 0$ are used to close the system of equations. The results show that in principle a spin-curvature interaction may lead to considerable deviations from geodesic motion, although in astrophysical situations of interest probably no large spin effects can be expected for values of spin consistent with a pole–dipole test-particle approximation. However, a significant cumulative effect may occur, e.g. in the inspiral of a spinning particle on to a rotating compact body, that would modify gravitational waves generated by such a system. A thorough literature review is included in the paper.

Key words: black hole physics – gravitation – relativity.

1 INTRODUCTION

The ever-growing evidence for collapsed cores in some galactic nuclei and stellar-size X-ray sources (Rees 1998) feeds an undying interest in physical processes around black holes, mainly in possible mechanisms for, and observable implications of, the interaction of rotating black holes with other bodies and their fields. Such interactions primarily involve the problem of motion in general relativity. The latter has a long history (e.g. Damour 1987) and a familiar solution in its simplest case (Infeld & Schild 1949; note, however, the problems discussed e.g. by Nevin 1995): free, non-gravitating ('test') point (i.e. structureless, monopole) particles move on geodesics.[1] On the other hand, the most complicated case is that in which the length-scales involved do not allow separation into 'body plus external universe' and the Einstein equations for a fully coupled system have to be solved.

An intermediate domain is spanned by the study of dynamics of (the systems of interacting) bodies that are 'isolated' (and non-radiating) but have non-trivial inner structure (are endowed with further multipoles) or/and have self-fields that cannot be neglected (e.g. Ehlers & Rudolph 1977; Dixon 1979; Thorne & Hartle 1985; Damour, Soffel & Xu 1991). Until now, only the motion of a test body carrying purely monopole and dipole (Papapetrou 1951) has been solved for particular solutions, mostly assuming the case free of non-gravitational torques. Although non-gravitational forces were also taken to be zero when the primary interest was in *orbits* (e.g. Corinaldesi & Papapetrou 1951; Micoulaut 1967; Rasband 1973; Tod, de Felice & Calvani 1976; Carmeli, Charach & Kaye 1977; Abramowicz & Calvani 1979; Plyatsko 1988; Suzuki & Maeda 1997), a *spin* behaviour has been examined in a force-free situation (e.g. Wilkins 1970; Mashhoon 1971; Apostolatos 1996) as well as with non-zero force (usually along a prescribed trajectory; see e.g. Fuchs 1983 or the references on gyroscopic precession given in Semerák 1996 and 1997). Both force and torque *are* present in the dynamics of *charged* pole–dipole test particles in gravitational plus electromagnetic fields (Dixon 1964; Künzle 1972; Hojman & Hojman 1977; Prasanna & Virbhadra 1989). Besides the single-particle treatments, Tafel (1980) proposed a kinetic model of an *ensemble* of (charged) spinning particles in self-consistent backgrounds, and Ray & Smalley (1982) investigated a *fluid* with an intrinsic spin.

Endowing the test body with spin may lead to interesting departures from geodesic motion when the gravitational background is sufficiently non-homogeneous (curved). More specifically, allowing for the dipole necessarily implies non-zero size of a body, and thus tidal forces come into play. The effects of the spin-curvature interaction were discussed notably by Wald (1972) and Barker & O'Connell (1979). The latter paper also reviews a more general spin-dependent *two*-body problem (both in classical and quantum versions) that must be treated when masses of the involved bodies become comparable and one cannot distinguish between the 'gravitational centre' and the 'test particle'; it also calculates corrections resulting from potential non-zero torsion and gives many references. [For concrete examples of spin effects in a Kerr(–Newman) field see the articles cited in Section 4].

Most recently, spin effects have been investigated as modulators of the gravitational waves generated by a coalescing binary system of neutron stars or/and black holes (Apostolatos et al. 1994; Kidder 1995). The gravitational waves produced by a spinning particle falling into (along the symmetry axis) or circulating

★ E-mail: semerak@mbox.troja.mff.cuni.cz

[1] Most results on geodesics in *black hole* space–times have been derived, reviewed or cited by Stewart & Walker (1973), Krivenko, Pyragas & Zhuk (1976), Sharp (1979), Chandrasekhar (1983), Dymnikova (1986) and Bičák, Semerák & Hadrava (1993).

around (in the equatorial plane of) a Kerr black hole have been calculated by Mino, Shibata & Tanaka (1996) and Tanaka et al. (1996). It has also been shown, by Suzuki & Maeda (1997) in Schwarzschild space–time, that the spin effect can make the test particle motion chaotic.

The present paper shows particular worldlines (of a general type) of free pole–dipole test particles in the Kerr space–time, found by numerical integration of the Mathisson–Papapetrou equations. Trajectories of particles with different values of spin are compared, to conclude that (i) in principle spin may influence the shape of a trajectory very strongly, but (ii) the spin values expected in astrophysical situations (which can be treated as test-particle motion) do not seem to be sufficient to create large effects; (iii) however, a significant secular effect may occur e.g. in the inspiral of a spinning particle on to a rotating compact body, which would modify the generated gravitational waves. (For a preliminary summary of the results, see Semerák 1999.) Note that the particles are assumed to have non-zero rest mass. For a treatment of *massless* pole–dipole particles (which simply follow the null geodesics of the space–time), see Mashhoon (1975), Bailyn & Ragusa (1977, 1981) or Duval & Fliche (1978).

Different 'spin supplementary conditions', used in the literature to fix the representative point of the particle, proved to imply *different* equations of motion (Barker & O'Connell 1974). We plan to visualize these differences in the second part of the paper, by comparing the trajectories obtained with different supplementary conditions.

We use geometrized units ($c = G = 1$) and the metric signature $(-+++)$, with Greek indices running from 0–3 and Latin indices from 1–3. Index-posed brackets mean antisymmetrization in the outer of the enclosed indices, according to '$[\mu\cdots\nu] = \frac{1}{2}(\mu\cdots\nu - \nu\cdots\mu)$'.

2 MATHISSON–PAPAPETROU (MP) EQUATIONS

In a space–time with metric $g_{\mu\nu}$, Christoffel symbols $\Gamma^{\mu}_{\rho\sigma}$ and the Riemann tensor $R^{\mu}_{\nu\rho\sigma} = 2(\Gamma^{\mu}_{\iota[\rho}\Gamma^{\iota}_{\sigma]\nu} - \Gamma^{\mu}_{\nu[\rho,\sigma]})$, we consider a classical test body (of positive rest mass) that is so small compared with the background curvature length-scale that all its multipoles beyond the dipole can be neglected. Free motion of such a 'pole–dipole particle', or 'torque-free gyroscope', is described by equations that seem effectively to be those first discussed in Frenkel's (1926) special-relativistic 'Electrodynamics of rotating electrons' (later Weyssenhoff & Raabe 1947a,b and Weyssenhoff 1947a,b also considered massless spin particles), then obtained for the linearized theory of gravitation by Mathisson (1937) and for full general relativity by Papapetrou (1951); the first general covariant derivations were given by Tulczyjew (1959), Taub (1964) and Dixon (1964; here also higher multipoles were included). The Mathisson–Papapetrou (MP) equations read[2]

$$(mu^{\mu} - u_{\sigma}\dot{S}^{\mu\sigma})^{\cdot} = -\frac{1}{2}R^{\mu}_{\nu\rho\sigma}u^{\nu}S^{\rho\sigma}, \tag{1}$$

$$\dot{S}^{\mu\nu} = 2u^{[\mu}\dot{S}^{\nu]\sigma}u_{\sigma}, \tag{2}$$

where m is a scalar parameter (the 'kinematical' or 'monopole' rest mass of a particle), the skew tensor $S^{\mu\nu}$ represents an internal angular momentum ('spin') of the particle, the tangent vector to the worldline of the particle u^{μ} is referred to as 'kinematical four-velocity', and the dot denotes absolute differentiation with respect to the proper time τ of the particle.

In terms of the total four-momentum of the particle,

$$p^{\mu} = mu^{\mu} - u_{\sigma}\dot{S}^{\mu\sigma}, \tag{3}$$

equations (1) and (2) can be rewritten as

$$\dot{p}^{\mu} = -\frac{1}{2}R^{\mu}_{\nu\rho\sigma}u^{\nu}S^{\rho\sigma}, \tag{4}$$

$$\dot{S}^{\mu\nu} = 2p^{[\mu}u^{\nu]}. \tag{5}$$

Generalization of the MP equations to the case of *charged* particles and non-zero electromagnetic field was achieved by Papapetrou & Urich (1955) (within special relativity the method by which to involve external forces was already given by Mathisson 1940), and then covariantly by Dixon (1964), Künzle (1972) and Hojman & Hojman (1977) by different approaches (cf. also Prasanna & Virbhadra 1989). Another possible generalization involves space–times with non-zero torsion (Hojman 1978 and references therein).

Useful consequences of the above equations involve

$$p_{\sigma}u^{\sigma} = -m, \tag{6}$$

$$\dot{p}_{\sigma}u^{\sigma} = 0, \tag{7}$$

$$\dot{u}_{\sigma}\dot{S}^{\mu\sigma} = \dot{u}_{\rho}u_{\sigma}\dot{S}^{\rho\sigma}u^{\mu}, \tag{8}$$

$$\dot{p}_{\sigma}\dot{S}^{\mu\sigma} = m^{-1}\dot{p}_{\rho}p_{\sigma}\dot{S}^{\rho\sigma}u^{\mu}, \tag{9}$$

$$(\mathcal{M}^2 - m^2)u^{\mu} = -u^{\iota}\dot{S}_{\sigma\iota}\dot{S}^{\mu\sigma}, \tag{10}$$

$$(\mathcal{M}^2 - m^2)p^{\mu} = -p^{\iota}\dot{S}_{\sigma\iota}\dot{S}^{\mu\sigma}, \tag{11}$$

$$\mathcal{M}^2u^{\mu} - mp^{\mu} = p_{\sigma}\dot{S}^{\mu\sigma}, \tag{12}$$

$$(\mathcal{M}^2 - m^2)\dot{S}^{\mu\nu} = \dot{S}^{\sigma\mu}\dot{S}_{\rho\sigma}\dot{S}^{\nu\rho}, \tag{13}$$

$$\begin{aligned}\mathcal{M}^2 - m^2 &= u^{\iota}\dot{S}_{\sigma\iota}p^{\sigma} = \frac{1}{2}\dot{S}_{\rho\sigma}\dot{S}^{\rho\sigma}\\ &= -u^{\iota}\dot{S}_{\sigma\iota}u_{\kappa}\dot{S}^{\sigma\kappa} = -\mathcal{U}^{\iota}\dot{S}_{\sigma\iota}\mathcal{U}_{\kappa}\dot{S}^{\sigma\kappa}\\ &= -m^{-1}u^{\iota}\dot{S}_{\sigma\iota}p_{\kappa}\dot{S}^{\sigma\kappa};\end{aligned} \tag{14}$$

here

$$\mathcal{M} = \sqrt{-p_{\sigma}p^{\sigma}} \tag{15}$$

is the 'dynamical', 'total' or 'effective' rest mass of the particle and $\mathcal{U}^{\mu} = p^{\mu}/\mathcal{M}$ is its 'dynamical four-velocity'. If $\mathcal{U}^{\mu} = u^{\mu}$, then $\mathcal{M} = m$.

Neither of the mass parameters need be a constant of motion, namely

$$\mathrm{d}m/\mathrm{d}\tau = \dot{m} = -\dot{u}_{\sigma}p^{\sigma} = \dot{u}_{\rho}u_{\sigma}\dot{S}^{\rho\sigma}, \tag{16}$$

$$\mathrm{d}\mathcal{M}/\mathrm{d}\tau = \dot{\mathcal{M}} = -\mathcal{U}_{\sigma}\dot{p}^{\sigma} = (m\mathcal{M})^{-1}\dot{p}_{\rho}p_{\sigma}\dot{S}^{\rho\sigma}. \tag{17}$$

However, the existence of integrals of motion is guaranteed when the background space–time has some symmetries (Dixon 1970): for each Killing field ξ^{μ}, one has

$$p_{\sigma}\xi^{\sigma} - \frac{1}{2}\xi_{\rho;\sigma}S^{\rho\sigma} = \text{constant} \tag{18}$$

(the semicolon stands for covariant differentiation). In certain

[2] Some works using the +2 signature cite equations (1) and (2) *exactly* as they were given in the original references (where the −2 signature was used), which results in the wrong signs of the terms containing u_{σ}. (Further confusion may arise from different sign conventions for $R^{\mu}_{\nu\rho\sigma}$ and $S^{\mu\nu}$.)

space–times other expressions may also be conserved, involving a Killing–Yano tensor field (Rüdiger 1981, 1983).

The equations (1) and (2), or (4) and (5), are three too few to determine u^μ (or p^μ) and $S^{\mu\nu}$, so one needs further conditions, specifying a reference point about which the momentum and spin of the particle are calculated. The latter is usually taken to be the centre of mass of the particle which, however, is not an invariant point of the body (it is frame-dependent; Møller 1949). Two rival conditions for its definition are usually imposed as the side constraints:

$$u_\sigma S^{\mu\sigma} = 0 \tag{19}$$

or

$$\mathcal{U}_\sigma S^{\mu\sigma} = 0. \tag{20}$$

The constraints (19) imply, in view of (8) and (16), that

$$\dot{u}_\sigma \dot{S}^{\mu\sigma} = 0, \tag{21}$$

$$\mathrm{d}m/\mathrm{d}\tau = 0; \tag{22}$$

the spin four-vector, defined by

$$s^\mu = \frac{1}{2}\epsilon^{\nu\mu}_{\rho\sigma} u_\nu S^{\rho\sigma} \tag{23}$$

($\epsilon^{\nu\mu}_{\rho\sigma}$ is the Levi–Civita tensor) and thus orthogonal to u^μ, $u_\sigma s^\sigma = 0$, is then Fermi-transported along the worldline of the particle,

$$\dot{s}^\mu = u^\mu \dot{u}_\sigma s^\sigma. \tag{24}$$

The other constraints (20) imply, in view of (9) and (17), that

$$\dot{\mathcal{U}}_\sigma \dot{S}^{\mu\sigma} = 0, \tag{25}$$

$$\mathrm{d}\mathcal{M}/\mathrm{d}\tau = 0 \tag{26}$$

(the latter assures that $\mathcal{U}^\mu$ remains time-like, $\mathcal{U}_\sigma \mathcal{U}^\sigma = -1$); the spin four-vector, in this case defined by

$$\mathcal{S}^\mu = \frac{1}{2}\epsilon^{\nu\mu}_{\rho\sigma} \mathcal{U}_\nu S^{\rho\sigma} \tag{27}$$

and thus orthogonal to $\mathcal{U}^\mu$ ($\mathcal{U}_\sigma \mathcal{S}^\sigma = 0$), is Fermi-transported along the integral curve of $\mathcal{U}^\mu$,

$$\dot{\mathcal{S}}^\mu = \mathcal{U}^\mu \dot{\mathcal{U}}_\sigma \mathcal{S}^\sigma. \tag{28}$$

Both definitions lead to

$$2s_\sigma s^\sigma = 2\mathcal{S}_\sigma \mathcal{S}^\sigma = S_{\rho\sigma} S^{\rho\sigma}, \tag{29}$$

and, regarding the transport laws (24) and (28), to

$$\mathrm{d}(s_\sigma s^\sigma)/\mathrm{d}\tau = \mathrm{d}(\mathcal{S}_\sigma \mathcal{S}^\sigma)/\mathrm{d}\tau = 0. \tag{30}$$

The conditions (19) were suggested by Mathisson (1937) (the idea had already been found in a special-relativistic treatment by Lanczos 1929), and then used, e.g., by Pirani (1956), Schiff (1960), Taub (1964), Wilkins (1970), Mashhoon (1971), Omote (1973), Rasband (1973), Ray & Smalley (1982), Prasanna & Virbhadra (1989), Aguirregabiria et al. (1996) and Apostolatos (1996).[3] Whereas they seem to be the most natural conditions for massless particles (Mashhoon 1975; Bailyn & Ragusa 1977; Duval & Fliche 1978), in the massive case they lead to a possibility of unphysical helical motions (Weyssenhoff & Raabe 1947a,b) as an effective consequence of a non-unique choice of the centre of mass (or 'center of gravity', Møller 1949) of the particle. Here we therefore adhere to the conditions (20), which were suggested by Tulczyjew (1959) (and matched the ideas developed by Synge 1935 and Pryce 1948 within special relativity), further justified by Dixon (1964), Beiglböck (1967), Madore (1969) and Schattner (1979a,b), and used, e.g., by Micoulaut (1967), Dixon (1970, and also in his following papers – see their review in Dixon 1979), Künzle (1972), Wald (1972, 1974), Tod et al. (1976), Hojman & Hojman (1977), Ehlers & Rudolph (1977), Tafel (1980), Rüdiger (1981), Mino, Shibata & Tanaka (1996) and Suzuki & Maeda (1997). We note, however, that recently Ragusa & Bailyn (1995) supported the original Mathisson's constraint by showing that it specifies the representative point of the body that *is* invariant (the same in any reference frame); they called it the 'center of trace'. See this reference, and also Schiff (1960), Bonazzola (1964), O'Connell (1974) and Barker & O'Connell (1974, 1979) (for massless particles, Bailyn & Ragusa 1981) for a discussion of the different supplementary conditions.

To determine the trajectory of the particle, one must know the tangent $u^\mu(\tau)$, which, however, can only be found indirectly from $p^\mu(\tau)$ and $S^{\mu\nu}(\tau)$. Imposing the constraints (20), we can rewrite the right-hand side of (12) as

$$p_\sigma \dot{S}^{\mu\sigma} = -\dot{p}_\sigma S^{\mu\sigma}. \tag{31}$$

Substituting for $\dot{p}_\sigma$ from (4) with u^ν once more expressed from (12) and (31), and then rewriting again the term containing $\dot{p}_\iota S^{\alpha\iota}$ according to the relation

$$R_{\sigma\alpha\beta\gamma} S^{\mu\sigma} S^{\alpha\iota} = R_{\sigma\alpha\beta\gamma} S^{\mu[\sigma} S^{\alpha]\iota} = \frac{1}{2} R_{\sigma\alpha\beta\gamma} S^{\alpha\sigma} S^{\mu\iota}, \tag{32}$$

induced by the antisymmetry of $S^{\mu\nu}$, one finds that

$$(4\mathcal{M}^2 - R_{\rho\alpha\beta\gamma} S^{\alpha\rho} S^{\beta\gamma}) \dot{p}_\sigma S^{\mu\sigma} = -2m S^{\mu\sigma} R_{\sigma\alpha\beta\gamma} p^\alpha S^{\beta\gamma}. \tag{33}$$

Equations (12), (31) and (33) yield the result

$$u^\mu = \frac{m}{\mathcal{M}} \left(\mathcal{U}^\mu + \frac{2 S^{\mu\nu} R_{\nu\iota\kappa\lambda} \mathcal{U}^\iota S^{\kappa\lambda}}{4\mathcal{M}^2 + R_{\alpha\beta\gamma\delta} S^{\alpha\beta} S^{\gamma\delta}} \right); \tag{34}$$

the general relation between u^μ and $\mathcal{U}^\mu$ was first obtained, for any multipole body, by Ehlers & Rudolph (1977). Note that in contrast to $\mathcal{U}^\mu$ the kinematical four-velocity u^μ may *not* be time-like everywhere. This circumstance, however, appears simply to indicate the limits of validity of the MP equations; namely, a spinning particle must have a certain minimum size (Møller 1949) which, for a sufficiently large spin or/and a sufficiently non-homogeneous field, may become incompatible with the pole–dipole approximation or with the test-body approach itself (Tod et al. 1976; Hojman & Hojman 1977). We will therefore check the character of u^μ within the integration of MP equations (see below) and will restrict ourselves to situations when the pole–dipole test-particle ideal is realizable, i.e. when one can treat the u^μ as the usual four-velocity, with $u_\sigma u^\sigma = -1$ ($\Rightarrow \dot{u}_\sigma u^\sigma = 0$). This normalization formula must be used to fix the parameter m in (34), because the latter is *not* a constant of motion in the case in which the spin condition (20) is employed.

[3] Corinaldesi & Papapetrou (1951) proposed a supplementary condition $S^{i0} = 0$, which is not covariant unless it is considered a special case of (19), given by a particular choice of u^μ (having $u_i = 0$). It was used e.g. by Prasanna & Kumar (1973).

3 SOLUTION OF THE MP EQUATIONS

It is the purpose of the present paper to find, by numerical integration of MP equations, the free motion of particular spinning particles in a given (Kerr) field. Let us give the initial conditions for the integration of equations (4)–(5) and (34) with respect to the local hypersurface-orthogonal observer (HOO), defined by a four-velocity $u^\mu_{\rm HOO}$, and with respect to his local orthonormal space triad (HOF) $\{e^\mu_i\}$. Denoting the relative dynamical velocity of a particle by $\hat{\mathcal{V}}^\mu$ and its relative spin with respect to the HOO by $\hat{\mathcal{S}}^\mu$ ($\hat{\mathcal{V}}_\sigma u^\sigma_{\rm HOO}=0$, $\hat{\mathcal{S}}_\sigma u^\sigma_{\rm HOO}=0$), one decomposes the dynamical four-velocity of the particle as

$$\mathcal{U}^\mu = \hat\Gamma(u^\mu_{\rm HOO} + \hat{\mathcal{V}}^\mu) \tag{35}$$

and its spin four-vector as

$$\mathcal{S}^\mu = \hat\Gamma(u^\mu_{\rm HOO}\,\hat{\mathcal{V}}_\nu\,\hat{\mathcal{S}}^\nu + \hat{\mathcal{S}}^\mu), \tag{36}$$

where $\hat\Gamma = -\mathcal{U}_\sigma u^\sigma_{\rm HOO} = (1-\hat{\mathcal{V}}^2)^{-1/2}$ is the relative boost factor and $\hat{\mathcal{V}}^2 = \hat{\mathcal{V}}_\sigma\hat{\mathcal{V}}^\sigma$.[4] The HOF components (represented by indices with hats) of $\hat{\mathcal{V}}^\mu$ and $\hat{\mathcal{S}}^\mu$ can be written as

$$\hat{\mathcal{V}}^{\hat\imath} = \hat{\mathcal{V}}(\cos\hat\alpha^{\rm v},\ \sin\hat\alpha^{\rm v}\cos\hat\beta^{\rm v},\ \sin\hat\alpha^{\rm v}\sin\hat\beta^{\rm v}), \tag{37}$$

$$\hat{\mathcal{S}}^{\hat\imath} = \hat{\mathcal{S}}(\cos\hat\alpha^{\rm s},\ \sin\hat\alpha^{\rm s}\cos\hat\beta^{\rm s},\ \sin\hat\alpha^{\rm s}\sin\hat\beta^{\rm s}), \tag{38}$$

where the angles $\hat\alpha$ and $\hat\beta$ specify the spatial direction locally.

In a given space–time, the integration of MP equations from a given initial point $x^\mu_{\rm in}$ starts from a specification of the initial values $\hat{\mathcal{V}}_{\rm in}$, $\hat\alpha^{\rm v}_{\rm in}$, $\hat\beta^{\rm v}_{\rm in}$, $\hat{\mathcal{S}}_{\rm in}/\mathcal{M}$, $\hat\alpha^{\rm s}_{\rm in}$ and $\hat\beta^{\rm s}_{\rm in}$, from which $\mathcal{U}^\mu_{\rm in}, \tilde{\mathcal{S}}^\mu_{\rm in} = \mathcal{S}^\mu_{\rm in}/\mathcal{M}$ and

$$\tilde{\mathcal{S}}^{\mu\nu}_{\rm in} = \mathcal{S}^{\mu\nu}_{\rm in}/\mathcal{M} = (\epsilon^{\mu\nu}_{\rho\sigma}\mathcal{U}^\rho\tilde{\mathcal{S}}^\sigma)_{\rm in} \tag{39}$$

are obtained. The trajectory is then found by numerical integration of equations (4)–(5), with recurring use of equation (34). In each cycle one calculates the instantaneous tangent

$$u^\mu = \frac{m}{\mathcal{M}}\left(\mathcal{U}^\mu + \frac{2\tilde{S}^{\mu\nu}R_{\nu\iota\kappa\lambda}\mathcal{U}^\iota\tilde{S}^{\kappa\lambda}}{4+R_{\alpha\beta\gamma\delta}\tilde{S}^{\alpha\beta}\tilde{S}^{\gamma\delta}}\right) \tag{40}$$

($m/\mathcal{M}$ follows from its normalization $u_\sigma u^\sigma=-1$) and then an elementary step

$$\mathrm{d}\mathcal{U}^\mu = -\left(\frac{1}{2}R^\mu_{\nu\rho\sigma}\tilde{S}^{\rho\sigma} + \Gamma^\mu_{\nu\sigma}\mathcal{U}^\sigma\right)u^\nu\,\mathrm{d}\tau, \tag{41}$$

$$\mathrm{d}\tilde{S}^{\mu\nu} = 2\left(\mathcal{U}^{[\mu}u^{\nu]} + \Gamma^{[\mu}_{\rho\sigma}\tilde{S}^{\nu]\rho}u^\sigma\right)\mathrm{d}\tau, \tag{42}$$

$$\mathrm{d}x^\mu = u^\mu\,\mathrm{d}\tau. \tag{43}$$

As the mass parameter of the background space–time (M) appears only as a scalefactor, one writes the code in a standard way in terms of dimensionless quantities, i.e. with $M=1$.

4 TRAJECTORIES OF SPINNING PARTICLES IN THE KERR FIELD

The MP equations have often been considered to deduce *spin* behaviour along prescribed orbits. Simple types of particle *motion* have also been studied analytically in the Schwarzschild or Kerr fields (e.g. Corinaldesi & Papapetrou 1951; Rasband 1973; Tod et al. 1976; Abramowicz & Calvani 1979). However, *actual trajectories* have only been computed (and figured) by Plyatsko (1988) (this monograph contains a thorough list of references), Apostolatos (1996) and Suzuki & Maeda (1997). We will find, in a Kerr field, the trajectories of particles with different spins, and compare them with those followed by non-spinning test particles (i.e. with geodesics starting from the respective initial conditions). Whereas the references given above mainly concentrated on azimuthal motion in the equatorial plane, we are instead interested in motion in the $(r,\ \theta)$ plane, in particular in the influence of the spin of the outgoing particles on collimation of their trajectories about the axis of symmetry (studied by Bičák et al. 1993).

We use the Boyer–Lindquist coordinates $x^\mu=(t,r,\theta,\phi)$ in which the Kerr metric takes the form (e.g. Misner, Thorne & Wheeler 1973)

$$\mathrm{d}s^2 = -\frac{\Delta\Sigma}{\mathcal{A}}\mathrm{d}t^2 + \frac{\mathcal{A}}{\Sigma}\sin^2\theta(\mathrm{d}\phi-\omega_{\rm K}\,\mathrm{d}t)^2 + \frac{\Sigma}{\Delta}\mathrm{d}r^2 + \Sigma\,\mathrm{d}\theta^2, \tag{44}$$

where

$$\Delta = r^2 - 2Mr + a^2, \qquad \Sigma = r^2 + a^2\cos^2\theta, \tag{45}$$

$$\mathcal{A} = (r^2+a^2)^2 - \Delta a^2\sin^2\theta, \qquad \omega_{\rm K} = 2Mar/\mathcal{A}\,, \tag{46}$$

and M and a are parameters (mass and specific angular momentum) of the Kerr solution. In Kerr space–time, the HOO is represented by an observer with zero angular momentum with respect to the symmetry axis, ZAMO, having

$$u^\mu_{\rm ZAMO} = \sqrt{\Delta^{-1}\Sigma^{-1}\mathcal{A}}\ \ (1,0,0,\omega_{\rm K}), \tag{47}$$

and the observer's local Cartesian triad by the 'locally non-rotating frame', LNRF, with basis vectors

$$e^\mu_{\hat r} = (0,\sqrt{\Delta/\Sigma},0,0), \tag{48}$$

$$e^\mu_{\hat\theta} = (0,0,1/\sqrt{\Sigma},0), \tag{49}$$

$$e^\mu_{\hat\phi} = (0,0,0,\sqrt{\Sigma/\mathcal{A}}\,\sin^{-1}\theta). \tag{50}$$

Christoffel symbols and the Riemann tensor of the Kerr geometry are listed in the Appendix.

The metric (44) is stationary and axisymmetric, having Killing vectors $\xi^\mu_{(t)}=\delta^\mu_t$ and $\xi^\mu_{(\phi)}=\delta^\mu_\phi$. According to (18), the total energy of the particle,

$$-E = p_t - \frac{1}{2}g_{t\rho,\sigma}S^{\rho\sigma}, \tag{51}$$

and its azimuthal angular momentum,

$$\Phi = p_\phi - \frac{1}{2}g_{\phi\rho,\sigma}S^{\rho\sigma}, \tag{52}$$

at infinity are constants of motion (Micoulaut 1967). However, they are not sufficient to determine a generous trajectory and we will instead integrate the MP equations directly according to the scheme (40)–(43).

4.1 Numerical results

We used the fourth-order Runge–Kutta method, with the step in

[4] In the opposite sense, the relative vector quantities can be obtained as rescaled projections of the corresponding four-vectors on to the three-space of the HOO – e.g. $\hat{\mathcal{S}}^\mu = \hat\Gamma^{-1}(\delta^\mu_\nu + u^\mu_{\rm HOO}u_{{\rm HOO}\nu})\mathcal{S}^\nu$.

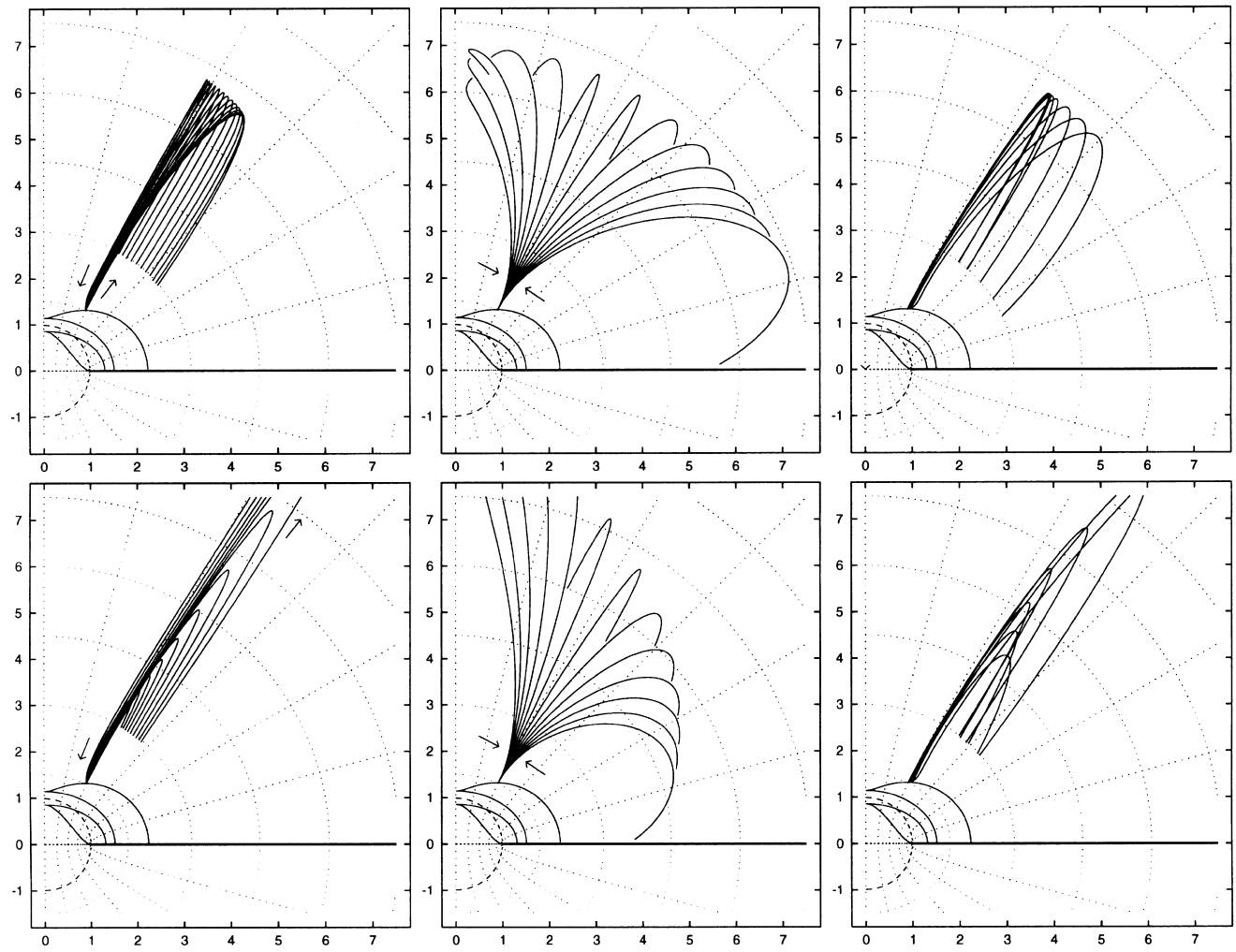

Figure 1. Trajectories of particles ejected with different $\hat{\mathcal{S}}^{\mu}_{\rm in}$ in the radial direction ($\hat{\alpha}^{\rm v}_{\rm in} = 0°$) from $r_{\rm in} = 1.5M$, $\theta_{\rm in} = 30°$, from a Kerr black hole with $a = 0.99M$. Top plots: fixed $E = 0.85\mathcal{M}$. Bottom plots: fixed $\hat{\mathcal{V}}_{\rm in} = 0.953094$. Left two plots – parallel/antiparallel initial spins ($\hat{\alpha}^{\rm s}_{\rm in} = 0°/180°$): respectively from left to right, six particles start with $\hat{\alpha}^{\rm s}_{\rm in} = 180°$ and $(\mathcal{M}\,M)^{-1}\,\hat{\mathcal{S}}_{\rm in} = 0.6, 0.5, 0.4, \ldots, 0.1$, the next one has zero spin (thus geodesic), and then six particles start with $\hat{\alpha}^{\rm s}_{\rm in} = 0°$ and $(\mathcal{M}\,M)^{-1}\,\hat{\mathcal{S}}_{\rm in} = 0.1, 0.2, 0.3, \ldots, 0.6$. In the top plot, $\hat{\mathcal{V}}_{\rm in} = 0.967902, 0.965974, 0.963865, 0.961552, 0.959009, 0.956202, 0.953094$ (geodesic), $0.949639, 0.945784, 0.941464, 0.936599, 0.931093, 0.924825$, while in the bottom plot, $E/\mathcal{M} = 0.6763, 0.7053, 0.7342, 0.7632, 0.7921, 0.8211, 0.8500$ (geodesic), $0.8789, 0.9079, 0.9368, 0.9658, 0.9947, 1.0237$, respectively; in both plots, $(\mathcal{M}\,M)^{-1}\Phi = -0.6037, -0.5031, -0.4025, -0.3019, -0.2012, -0.1006, 0.0000$ (geodesic), $0.1006, 0.2012, \ldots, 0.6037$. Middle pair of plots – transverse initial spins ($\hat{\alpha}^{\rm s}_{\rm in} = 90°$) lying in the sheet and pointing in the $(+\theta/-\theta)$ – direction ($\hat{\beta}^{\rm s}_{\rm in} = 0°/180°$): respectively from left to right, six particles start with $\hat{\beta}^{\rm s}_{\rm in} = 0°$ and $(\mathcal{M}\,M)^{-1}\,\hat{\mathcal{S}}_{\rm in} = 0.6, 0.5, 0.4, \ldots, 0.1$, the next one has zero spin (the same geodesic as in the left plots), and then six particles start with $\hat{\beta}^{\rm s}_{\rm in} = 180°$ and $(\mathcal{M}\,M)^{-1}\,\hat{\mathcal{S}}_{\rm in} = 0.1, 0.2, 0.3, \ldots, 0.6$. In the top plot, $\hat{\mathcal{V}}_{\rm in} = 0.944149, 0.945599, 0.947064, 0.948545, 0.950042, 0.951558, 0.953094$ (geodesic), $0.954652, 0.956235, 0.957847, 0.959489, 0.961168, 0.962888$, and $(\mathcal{M}\,M)^{-1}\Phi = -0.6000, -0.5129, -0.4214, -0.3249, -0.2229, -0.1149, 0.0000$ (geodesic), $0.1225, 0.2536, 0.3947, 0.5471, 0.7129, 0.8943$, while in the bottom plot, $E/\mathcal{M} = 0.9321, 0.9184, 0.9047, 0.8910, 0.8774, 0.8637, 0.8500$ (geodesic), $0.8363, 0.8226, 0.8090, 0.7953, 0.7816, 0.7679$, and $(\mathcal{M}\,M)^{-1}\Phi = -0.7111, -0.5926, -0.4741, -0.3556, -0.2370, -0.1185, 0.0000$ (geodesic), $0.1185, 0.2370, \ldots, 0.7111$, respectively. Right two plots – transverse initial spins ($\hat{\alpha}^{\rm s}_{\rm in} = 90°$) perpendicular to the sheet and pointing in the $(+\phi/-\phi)$ – direction ($\hat{\beta}^{\rm s}_{\rm in} = 90°/270°$). In the top plot, two particles start with $\hat{\beta}^{\rm s}_{\rm in} = 270°$ and $(\mathcal{M}\,M)^{-1}\,\hat{\mathcal{S}}_{\rm in} = 0.2, 0.1$, one particle has zero spin (the 'reference' geodesic), and then four particles start with $\hat{\beta}^{\rm s}_{\rm in} = 90°$ and $(\mathcal{M}\,M)^{-1}\,\hat{\mathcal{S}}_{\rm in} = 0.1, 0.2, 0.3, 0.4$ (compared with the left and middle pairs of plots, six paths are missing, the u^{μ} of which were space-like near the starting points); $\hat{\mathcal{V}}_{\rm in} = 0.958261, 0.955634, 0.953094$ (geodesic), $0.950625, 0.948218, 0.945865, 0.943560$, and $(\mathcal{M}\,M)^{-1}\Phi = -0.0123, -0.0058, 0.0000$ (geodesic), $0.0052, 0.0099, 0.0142, 0.0181$, respectively; the trajectories of the last five particles are more and more deflected towards the equatorial plane, the second one moves very slightly to the left of the third (the geodesic) and the first one a little to the left of the fourth. In the bottom plot, three particles start with $\hat{\beta}^{\rm s}_{\rm in} = 270°$ and $(\mathcal{M}\,M)^{-1}\,\hat{\mathcal{S}}_{\rm in} = 0.3, 0.2, 0.1$, one particle has zero spin (the geodesic), and then three particles start with $\hat{\beta}^{\rm s}_{\rm in} = 90°$ and $(\mathcal{M}\,M)^{-1}\,\hat{\mathcal{S}}_{\rm in} = 0.1, 0.2, 0.3$ (again the missing ones started as space-like); $E/\mathcal{M} = 0.7836, 0.8057, 0.8279, 0.8500$ (geodesic), $0.8721, 0.8943, 0.9164$, and $(\mathcal{M}\,M)^{-1}\Phi = -0.0164, -0.0110, -0.0055, 0.0000$ (geodesic), $0.0055, 0.0110, 0.0164$, respectively; the trajectories can be identified according to their energies – those with greater E turn farther from the centre, the geodesic orbit making the most narrow loop.

proper time τ chosen so that the proper spatial integration step $\sqrt{g_{ij}\,\mathrm{d}x^i\,\mathrm{d}x^j}$ is $M/100$ along the trajectories. Occasional control runs with a 10 times shorter step, and also those using a simple Euler method with a 100 times shorter step, agreed precisely.

We present here several figures that show trajectories projected on to the meridional plane of the Kerr–Schild coordinates $\rho = \sqrt{r^2 + a^2}\sin\theta$ and $z = r\cos\theta$. The values are given in units of M along both axes. The Boyer–Lindquist mesh (the lines of

$r =$ constant and $\theta =$ constant) is illustrated by dotted lines in all plots (the latitudes indicated are $\theta = 0°$, 15°, …, 90°). The region $z > 0$ corresponds to the $(r > 0)$ sheet of the manifold; also a small piece of the $(r < 0)$ sheet is shown $(z < 0)$, where the gravitational field acts in an exactly reverse manner (thus there are neither static limits nor horizons there). The two regions can communicate nowhere except through the $(r = 0)$ surface $(\rho < a$, $z = 0)$; the thick lines going to the right from the source (the Kerr ring singularity), which is just a point at $\rho = a$, $z = 0$ $(r = 0$, $\theta = 90°)$, indicate that there is no connection through the equatorial planes – the pictures end there from both sides. The source ring is spanned by a spherical region $\rho^2 + z^2 < a^2$ $(r^2 < a^2 \cos^2\theta)$, shown by dashed lines, which is the only part of Kerr space–time where momentarily static particles (if they really can exist there) are pulled upwards. The static limit surfaces $(r = M \pm \sqrt{M^2 - a^2\cos^2\theta})$ are represented by solid lines; the inner static limits lead to the singularities. In Figs 1 and 2 (with a Kerr black hole of $a = 0.99M$) the horizons (at $r = M \pm \sqrt{M^2 - a^2}$) are also shown by solid lines.

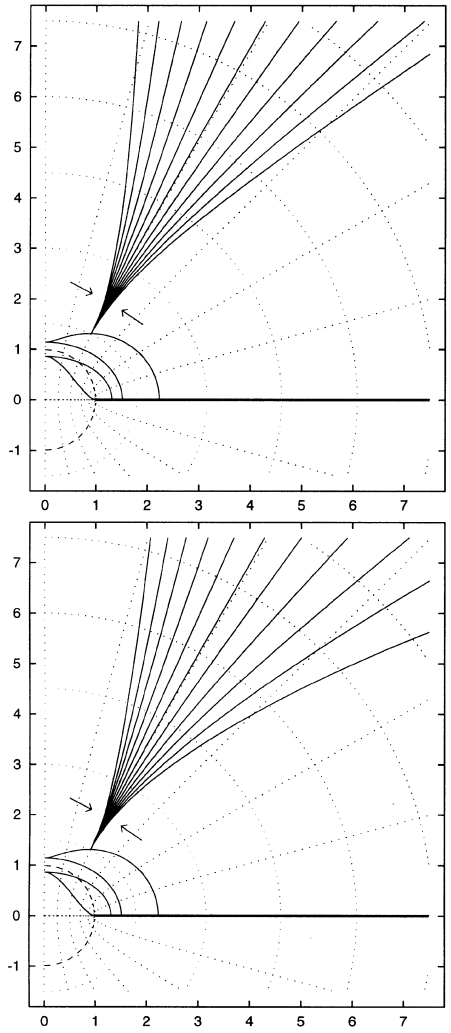

Figure 2. A more energetic counterpart of the middle two panels of Fig. 1; the particles with $(\mathcal{M}M)^{-1}\hat{\mathcal{S}}_{\rm in} = 0.6$ are not present, however, because they would start as space-like. Top plot: fixed $E = 1.05\mathcal{M}$; starting speeds are $\hat{\mathcal{V}}_{\rm in} = 0.963601$, 0.964751, 0.965916, 0.967098, 0.968297, 0.969517 (geodesic), 0.970760, 0.972029, 0.973328, 0.974662, 0.976038, and $(\mathcal{M}M)^{-1}\Phi = -0.7596$, −0.6271, −0.4861, −0.3355, −0.1740, 0.0000 (geodesic), 0.1884, 0.3937, 0.6189, 0.8680, 1.1466, respectively, as in Fig. 1. Bottom plot: fixed $\hat{\mathcal{V}}_{\rm in} = 0.969517$; energies are $E/\mathcal{M} = 1.1544$, 1.1335, 1.1126, 1.0917, 1.0709, 1.0500 (geodesic), 1.0291, 1.0083, 0.9874, 0.9665, 0.9456, and $(\mathcal{M}M)^{-1}\Phi = -0.9043$, −0.7234, −0.5426, −0.3617, −0.1809, 0.0000 (geodesic), 0.1809, 0.3617, …, 0.9043, again in the same order as in Fig. 1.

Fig. 1 brings trajectories of particles ejected with several different magnitudes $\hat{\mathcal{S}}_{\rm in}$ of the initial spin radially outwards $(\hat{\alpha}^{\rm v}_{\rm in} = 0°)$ from the LNRF at $r_{\rm in} = 1.5M$, $\theta_{\rm in} = 30°$, from a Kerr black hole with $a = 0.99M$. In the top three plots, all particles have the same total energy at infinity, $E = 0.85\mathcal{M}$, whereas in the bottom three plots, they have the same initial dynamical speed, $\hat{\mathcal{V}}_{\rm in} = 0.953094$. In the left two plots, the initial spins $\hat{\mathcal{S}}^{\mu}_{\rm in}$ are parallel/antiparallel to the initial dynamical velocity $\hat{\mathcal{V}}^{\mu}_{\rm in}$; in the middle two plots, $\hat{\mathcal{S}}^{\mu}_{\rm in}$ are perpendicular to $\hat{\mathcal{V}}^{\mu}_{\rm in}$ and lying in the plane of the sheet; in the right two plots, $\hat{\mathcal{S}}^{\mu}_{\rm in}$ are perpendicular to $\hat{\mathcal{V}}^{\mu}_{\rm in}$ and also to the sheet. Fig. 2 is a more energetic counterpart of the middle two plots in Fig. 1, with fixed $E = 1.05\mathcal{M}$ in the top plot and $\hat{\mathcal{V}}_{\rm in} = 0.969517$ in the bottom plot. The figures may be compared with fig. 2 of Bičák et al. (1993), where *spinless* particles were ejected radially with different velocities (and energies) from the same centre. Note that it is very important in the above figures that the central hole rotates: *all* the trajectories shown would be strictly radial in the Schwarzschild background.

Figs 3 and 4, on the other hand, are counterparts of fig. 12 in Bičák et al. (1993), where a fan of parabolic spinless particles was ejected from above the inside of a Kerr ring singularity of $a = 2M$. The trajectories, the tangents of which spanned 180° initially, were accelerated in the vertical direction and collimated into a much smaller angle by the central 'repulsive' region of the space–time. To see how this result would change for spinning particles, we take here the two marginal paths of the fan (given by $\hat{\alpha}^{\rm v}_{\rm in} = 90°$) – that starting to the left $(\hat{\beta}^{\rm v}_{\rm in} = 180°)$ and that starting to the right $(\hat{\beta}^{\rm v}_{\rm in} = 0°)$ – and find their shapes for different initial spins imposed on the particles. Fig. 3 shows trajectories of particles ejected in latitudinal directions $(\hat{\alpha}^{\rm v}_{\rm in} = 90°$, $\hat{\beta}^{\rm v}_{\rm in} = 0°, 180°)$ from the LNRF at $r_{\rm in} = 0.04M$, $\theta_{\rm in} = 20°$, from a Kerr naked singularity with $a = 2M$. In the top three plots, all particles have $E = \mathcal{M}$, whereas in the bottom three plots, they all start with $\hat{\mathcal{V}}_{\rm in} = 0.150264$. Initial spins $\hat{\mathcal{S}}^{\mu}_{\rm in}$ point upwards $(\hat{\alpha}^{\rm s}_{\rm in} = 0°)$ in the left two plots, downwards $(\hat{\alpha}^{\rm s}_{\rm in} = 180°)$ in the middle two plots, and to the left $(\hat{\alpha}^{\rm s}_{\rm in} = 90°$, $\hat{\beta}^{\rm s}_{\rm in} = 180°)$ in the right two plots. Fig. 4 is a continuation of Fig. 3; here the $\hat{\mathcal{S}}^{\mu}_{\rm in}$ point to the right $(\hat{\alpha}^{\rm s}_{\rm in} = 90°$, $\hat{\beta}^{\rm s}_{\rm in} = 0°)$ in the left two plots, towards the reader $(\hat{\alpha}^{\rm s}_{\rm in} = 90°$, $\hat{\beta}^{\rm s}_{\rm in} = 270°)$ in the middle two plots, and away from the reader $(\hat{\alpha}^{\rm s}_{\rm in} = 90°$, $\hat{\beta}^{\rm s}_{\rm in} = 90°)$ in the right two plots.

Fig. 5 shows trajectories of particles released from rest ($\hat{\mathcal{V}}_{\rm in} = 0$) from $r < 0$ near a Kerr ring singularity with $a = 2M$. In the left plot, they start from $r_{\rm in} = -0.8M$, $\theta_{\rm in} = 40°$, with the initial spins pointing along/against the local radial direction $(\hat{\alpha}^{\rm s}_{\rm in} = 0°/180°)$; in the right plot, they start from $r_{\rm in} = -0.7M$, $\theta_{\rm in} = 50°$, with the initial spins pointing along/against the local latitudinal direction $(\hat{\alpha}^{\rm s}_{\rm in} = 90°$ and $\hat{\beta}^{\rm s}_{\rm in} = 0°/180°)$.

The figures confirm that the spin-curvature effect strengthens with spin and with non-homogeneity of the background field, and also with decreasing relative amount of total energy E resulting from translational motion. With given spin, the pole–dipole test-particle approximation is better maintainable (u^{μ} remains rather time-like) for slow particles. The spin effect is best seen on low-energy particles travelling outwards (outgoing) from the vicinity of the source. Inward-travelling (ingoing) trajectories are strongly

deflected only very close to the centre where, however, the approximation usually breaks down anyway. For large spins (of the order of $\mathcal{M}M$) the orbits are often very complicated near the centre (though still in the region where u^μ is time-like). In the figures shown here, we followed outgoing particles with mild energies, $E = (0.67\text{–}1.15)\mathcal{M}$, and with spins $\hat{\mathcal{S}}_{\rm in} \leqslant 0.6\mathcal{M}M$, the trajectories of which still tend to have quite intuitive shapes. We often show only (ascending) parts of the orbits, which need not indicate that the approximation breaks down at the end-points (such cases are pointed out), but rather that we want the pictures to remain clear.

The spin contributes to the constants of motion (51,52) – in

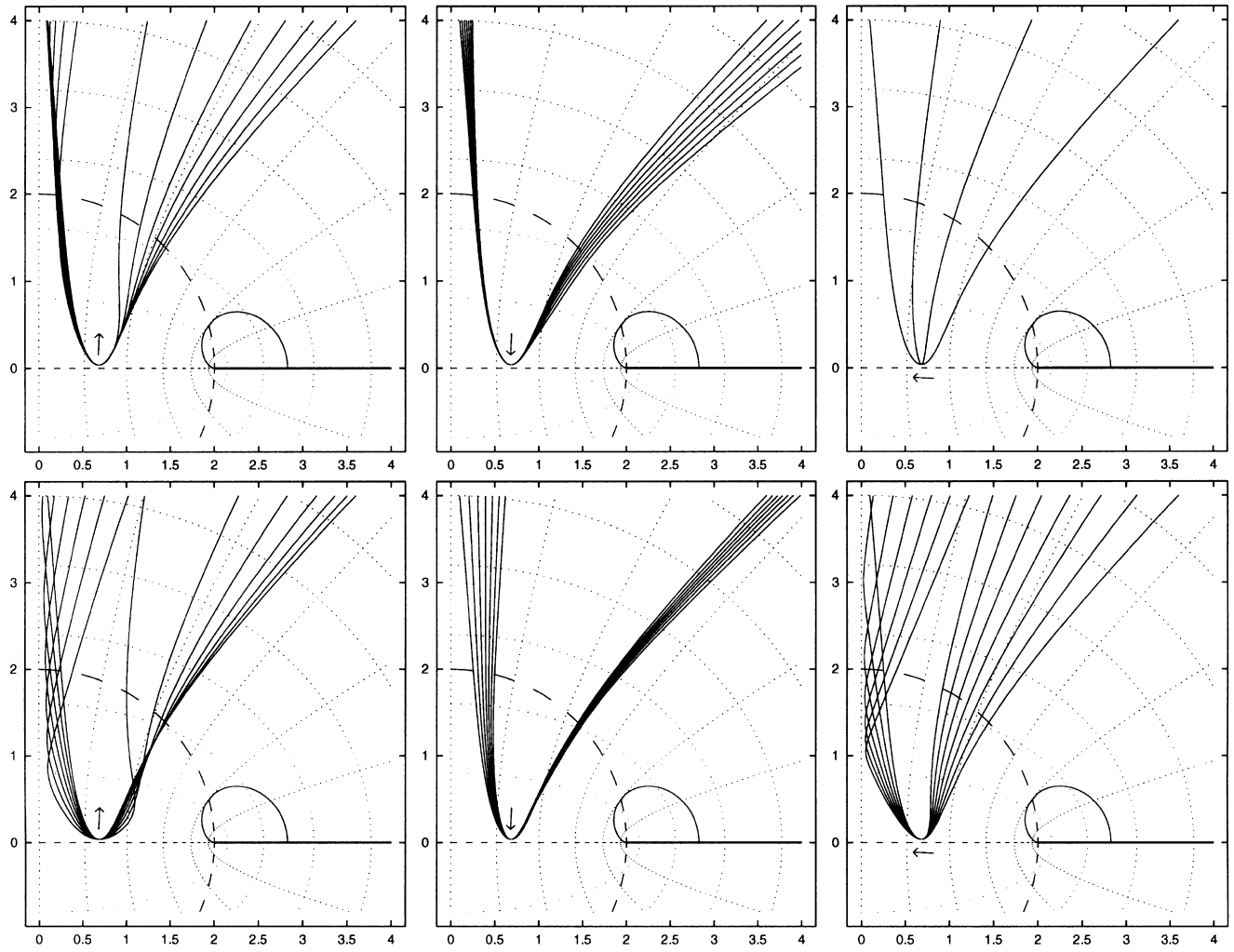

Figure 3. Trajectories of particles ejected in latitudinal directions ($\hat{\alpha}^{\rm v}_{\rm in} = 90°$, $\hat{\beta}^{\rm v}_{\rm in} = 0°, 180°$) from $r_{\rm in} = 0.04M$, $\theta_{\rm in} = 20°$, from a Kerr naked singularity with $a = 2M$. Top plots: fixed $E = \mathcal{M}$. Bottom plots: $\hat{\mathcal{V}}_{\rm in} = 0.150264$. Left two plots – initial spins pointing upwards ($\hat{\alpha}^{\rm s}_{\rm in} = 0°$): respectively from left to right (as taken where trajectories leave the plot), seven particles start to the left ($\hat{\beta}^{\rm v}_{\rm in} = 180°$), with $(\mathcal{M}M)^{-1}\,\hat{\mathcal{S}}_{\rm in} = 0.1$, 0.0 (geodesic), 0.2, …, 0.6, and seven to the right ($\hat{\beta}^{\rm v}_{\rm in} = 0°$), with $(\mathcal{M}M)^{-1}\,\hat{\mathcal{S}}_{\rm in} = 0.6$, 0.5, 0.4, …, 0.0 (geodesic); in the top plot, $\hat{\mathcal{V}}_{\rm in} = 0.141499$, 0.150264 (geodesic), 0.132165, 0.122134, 0.111216, 0.099119, 0.085343; 0.085343, 0.099119, …, 0.132165, 0.141499, 0.150264 (geodesic), and $(\mathcal{M}M)^{-1}\Phi = 0.1025$, 0.0000 (geodesic), 0.2044, 0.3058, 0.4067, 0.5071, 0.6070; 0.6070, 0.5071, …, 0.2044, 0.1025, 0.0000 (geodesic), while in the bottom plot, $E/\mathcal{M} = 1.0013$, 1.0000 (geodesic), 1.0026, 1.0039, 1.0052, 1.0065, 1.0079; 1.0079, 1.0065, …, 1.0026, 1.0013, 1.0000 (geodesic), and $(\mathcal{M}M)^{-1}\Phi = 0.1027$, 0.0000 (geodesic), 0.2055, 0.3082, 0.4110, 0.5137, 0.6165; 0.6165, 0.5137, …, 0.2055, 0.1027, 0.0000 (geodesic), respectively. Middle two plots – initial spins pointing downwards ($\hat{\alpha}^{\rm s}_{\rm in} = 180°$): respectively from left to right, again seven particles start to the left, with $(\mathcal{M}M)^{-1}\,\hat{\mathcal{S}}_{\rm in} = 0.0$ (geodesic), 0.1, …, 0.6, and seven to the right, with $(\mathcal{M}M)^{-1}\,\hat{\mathcal{S}}_{\rm in} = 0.0$ (geodesic), 0.1, …, 0.6; in the top plot, $\hat{\mathcal{V}}_{\rm in} = 0.150264$ (geodesic), 0.158557, 0.166447, 0.173989, 0.181228, 0.188197, 0.194926; 0.150264 (geodesic), 0.158557, …, 0.194926, and $(\mathcal{M}M)^{-1}\Phi = 0.0000$ (geodesic), −0.1030, −0.2066, −0.3107, −0.4154, −0.5206, −0.6264; 0.0000 (geodesic), −0.1030, …, −0.6264, while in the bottom plot, $E/\mathcal{M}$=1.0000 (geodesic), 0.9987, 0.9974, 0.9961, 0.9948, 0.9935, 0.9921; 1.0000 (geodesic), 0.9987, …, 0.9921, and $(\mathcal{M}M)^{-1}\Phi = 0.0000$ (geodesic), −0.1027, −0.2055, −0.3082, −0.4110, −0.5137, −0.6165; 0.0000 (geodesic), −0.1027, …, −0.6165, respectively. Right two plots – initial spins pointing to the left ($\hat{\alpha}^{\rm s}_{\rm in} = 90°$, $\hat{\beta}^{\rm s}_{\rm in} = 180°$): in the top plot, two particles start to the left (respectively from left to right, as taken where trajectories leave the plot), with $(\mathcal{M}M)^{-1}\,\hat{\mathcal{S}}_{\rm in} = 0.1$, 0.0 (geodesic), and two to the right, with $(\mathcal{M}M)^{-1}\,\hat{\mathcal{S}}_{\rm in} = 0.0$ (geodesic), 0.1 (larger spins cannot be considered here, because for $\hat{\mathcal{S}}_{\rm in} > 0.111627\mathcal{M}M$ one always obtains $E > \mathcal{M}$, irrespective of the value of $\hat{\mathcal{V}}_{\rm in}$); $\hat{\mathcal{V}}_{\rm in} = 0.048869$, 0.150264 (geodesic), 0.150264 (geodesic), 0.048869, and $(\mathcal{M}M)^{-1}\Phi = 0.0031$, 0.0000 (geodesic), 0.0000 (geodesic), 0.0031, respectively; in the bottom plot, seven particles start to the left, with $(\mathcal{M}M)^{-1}\,\hat{\mathcal{S}}_{\rm in} = 0.0$ (geodesic), 0.1, …, 0.6, and seven to the right, with $(\mathcal{M}M)^{-1}\,\hat{\mathcal{S}}_{\rm in} = 0.6$, 0.5, …, 0.0 (geodesic); $E/\mathcal{M} = 1.0000$ (geodesic), 1.0102, 1.0203, 1.0305, 1.0407, 1.0509, 1.0610; 1.0610, 1.0509, …, 1.0000 (geodesic), and $(\mathcal{M}M)^{-1}\Phi = 0.0000$ (geodesic), 0.0031, 0.0062, 0.0093, 0.0124, 0.0155, 0.0186; 0.0186, 0.0155, …, 0.0000 (geodesic), respectively.

general one obtains different Es and Φs when fixing the initial velocity $\hat{\mathcal{V}}^{\hat{\imath}}_{\rm in}$ [also $(a, x^{\mu}_{\rm in})$] and choosing different initial spins $\hat{\mathcal{S}}^{\hat{\imath}}_{\rm in}$. On the other hand, to have uniform prescribed E (or Φ), one must choose different initial velocities for different initial spins. Both the values of $\hat{\mathcal{V}}^{\hat{\imath}}_{\rm in}$ and those of E and Φ, of course, strongly influence the shape of the trajectories. In order to demonstrate that the effects observed do *not* arise purely because of different choices of the local or global energetic characteristics for different orbits, each column of the panels in the figures consists of two plots. In the top one, all particles have the same energy E (but different initial speeds), whereas in the bottom one they have the same initial speed $\hat{\mathcal{V}}_{\rm in}$ (and different E).

The figures are consistent with the observation following from equations (4) and (27), namely that at a given point the spin-curvature effect changes sign when the spin itself ($\mathcal{S}^{\mu}$) is turned over. As expected, no simple answer can be given to the particular question of whether the collimation effects of the Kerr field, studied on spinless particles by Bičák et al. (1993), are stronger or

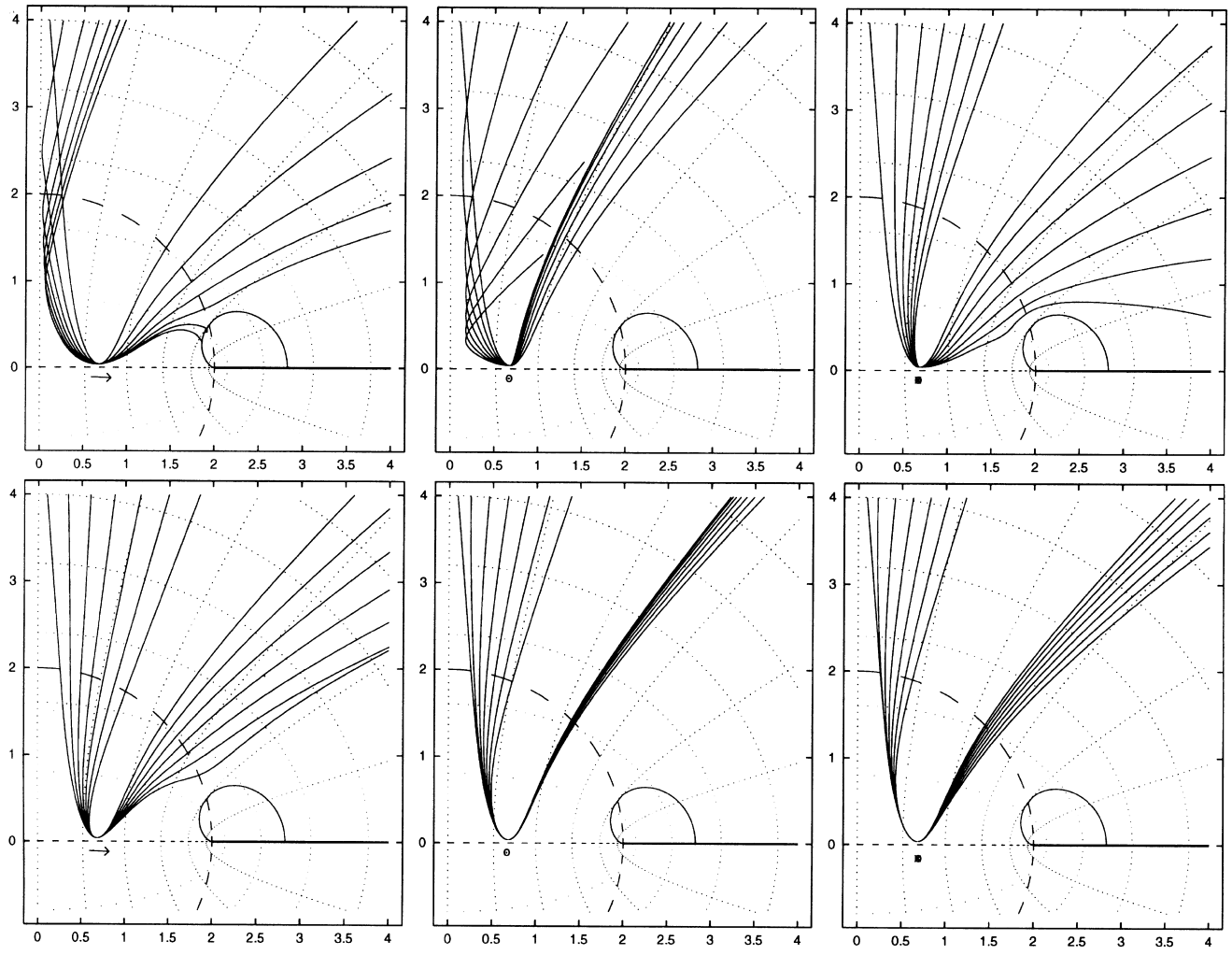

Figure 4. Continuation of Fig. 3 with different directions of the initial spin $\hat{\mathcal{S}}^{\mu}_{\rm in}$. Left two plots – initial spins pointing to the right ($\hat{\alpha}^{\rm s}_{\rm in} = 90°$, $\hat{\beta}^{\rm s}_{\rm in} = 0°$): respectively from left to right (in the top plot, as taken where the trajectories leave it), seven particles start to the left, with $(\mathcal{M}\,M)^{-1}\,\hat{\mathcal{S}}_{\rm in} = 0.0$ (geodesic), 0.1, …, 0.6, and seven to the right, with $(\mathcal{M}\,M)^{-1}\,\hat{\mathcal{S}}_{\rm in} = 0.0$ (geodesic), 0.1, …, 0.6; in the top plot, $\hat{\mathcal{V}}_{\rm in} = 0.150264$ (geodesic), 0.205338, 0.247317, 0.282148, 0.312268, 0.338965, 0.363023; 0.150264 (geodesic), 0.205338, …, 0.363023 (the last two trajectories are stopped near the ergosurface, where they become space-like), and $(\mathcal{M}\,M)^{-1}\Phi = 0.0000$ (geodesic), −0.0031, −0.0062, −0.0093, −0.0124, −0.0155, −0.0186; 0.0000 (geodesic), −0.0031, …, −0.0186, respectively; in the bottom plot, $E/\mathcal{M} = 1.0000$ (geodesic), 0.9898, 0.9797, 0.9695, 0.9593, 0.9491, 0.9390; 1.0000 (geodesic), 0.9898, …, 0.9390, and the angular momenta are the same as in the top plot. Middle two plots – initial spins pointing towards the reader ($\hat{\alpha}^{\rm s}_{\rm in} = 90°$, $\hat{\beta}^{\rm s}_{\rm in} = 270°$): respectively from left to right (in the top plot, as taken where the trajectories leave it or are stopped for lucidity), seven particles start to the left, with $(\mathcal{M}\,M)^{-1}\,\hat{\mathcal{S}}_{\rm in} = 0.0$ (geodesic), 0.1, …, 0.6, and seven to the right, with $(\mathcal{M}\,M)^{-1}\,\hat{\mathcal{S}}_{\rm in} = 0.6$, 0.5, …, 0.0 (geodesic); in the top plot, $\hat{\mathcal{V}}_{\rm in} = 0.150264$ (geodesic), 0.183389, 0.222511, 0.267143, 0.316750, 0.371040, 0.430212; 0.054618, 0.062458, 0.072427, 0.085256, 0.101858, 0.123237, 0.150264 (geodesic), and $(\mathcal{M}\,M)^{-1}\Phi = 0.0000$ (geodesic), −0.0013, −0.0033, −0.0061, −0.0099, −0.0151, −0.0222; 0.0023, 0.0022, 0.0020, 0.0018, 0.0014, 0.0009, 0.0000 (geodesic), respectively; in the bottom plot, $E/\mathcal{M} = 1.0000$ (geodesic), 0.9954, 0.9908, 0.9861, 0.9815, 0.9769, 0.9723; 1.0277, 1.0231, 1.0185, 1.0139, 1.0092, 1.0046, 1.0000 (geodesic), and $(\mathcal{M}\,M)^{-1}\Phi = 0.0000$ (geodesic), −0.0011, −0.0022, −0.0032, −0.0043, −0.0054, −0.0065; 0.0065, 0.0054, …, 0.0000 (geodesic), respectively. Right two plots – initial spins pointing away from the reader ($\hat{\alpha}^{\rm s}_{\rm in} = 90°$, $\hat{\beta}^{\rm s}_{\rm in} = 90°$): respectively from left to right, again seven particles start to the left, with $(\mathcal{M}\,M)^{-1}\,\hat{\mathcal{S}}_{\rm in} = 0.0$ (geodesic), 0.1, …, 0.6, and seven to the right, with $(\mathcal{M}\,M)^{-1}\,\hat{\mathcal{S}}_{\rm in} = 0.0$ (geodesic), 0.1, …, 0.6; the values specific to the top and the bottom plots are exactly the same as those given for the middle pair, but those values that corresponded to particles starting to the left now belong to those starting to the right and vice versa.

weaker for particles with spin: this depends on the interplay of several factors, the influence of spin itself depends mainly on the relative orientation of the spin of a particle and of that of the centre.

Regarding the values of E which a particle with fixed $\hat{\mathcal{V}}_{\rm in}$ gains (at a given point of a given space–time) for different $\hat{\mathcal{S}}^{\mu}_{\rm in}$, one can see the well-known fact that parallel spins repel and antiparallel attract each other. Let us note that the repulsive force between aligned spins can even compensate for scalar gravitational attraction and prevent a pair of rotating bodies from falling on each other. For example, Wald (1974) learned that it is not possible to turn the extreme Kerr–Newman black hole into a naked singularity by dropping in a test body with large aligned spin along the symmetry axis, because the body cannot enter the hole owing to the spin–spin repulsion (cf. Caderni & Calvani 1979, and Calvani 1980 for the case of equatorial injection). The first *exact* solution, which describes two objects held apart thus in equilibrium, was obtained by Dietz & Hoenselaers (1982) by addition of spin to the sources of the static solution known as Curzon–Chazy particles. By analysing the 'double Kerr' solution, Dietz & Hoenselaers (1985) found that two parallel Kerr centres on a common axis may also be in balance, although only when they are hyperextreme ($a > M$); a similar analysis of the double Kerr–NUT solution is given by Leterier & Oliveira (1998). The spin effects seem also to operate in the same manner in an exact solution by Manko, Martín & Ruiz (1994), representing the exterior field of two arbitrary (anti-)aligned Kerr–*Newman* sources. In the special case of two identical Kerr–Newman centres with opposite spins, the only equilibrium has been reached when the masses of the sources are equal to the charges, irrespectively of their rotation (Bretón & Manko 1995). In this situation the rotation weakens the scalar gravity of each of the bodies, which, however, is compensated for by an increasing attraction of their antiparallel spins. Pfister & Schedel (1987) showed, in the weak-field limit, that the spin–spin interaction acts similarly between two corotating spherical mass shells.

In a recent boom in gravitational wave detection, theory mainly attempts to say which structure of the wavefronts one should await, which involves a detailed study of potential sources. Among these, the most prominent is an inspiral of two very compact objects. Late stages of collision are being analysed by numerous authors, either numerically or in some approximation. For example, if the masses of the objects were sufficiently different, the test-motion approach could provide reasonable estimates. Modification of the wavefronts resulting from spin effects has been treated in several references (see Introduction). The case of a spinning particle falling along the symmetry axis of a Kerr black hole was considered by Mino et al. (1996) and that of a particle orbiting in the equatorial plane by Tanaka et al. (1996). We show here that the inspiral along an approximately *polar* trajectory is also sensitive to the spins involved. In Fig. 6, three particles with different initial spins, but with the same energy (left plot) or initial velocity (right plot), fall towards an extreme Kerr hole. Even though the particles start as close as at $r = 8M$ and make just one complete orbit, their trajectories diverge enough to hit the horizon at very different locations. It thus seems clear that for a realistic inspiral, involving many more revolutions, even a spin much less than $\hat{\mathcal{S}} = 0.5\mathcal{M}\,M$ (used in the figure) can have a

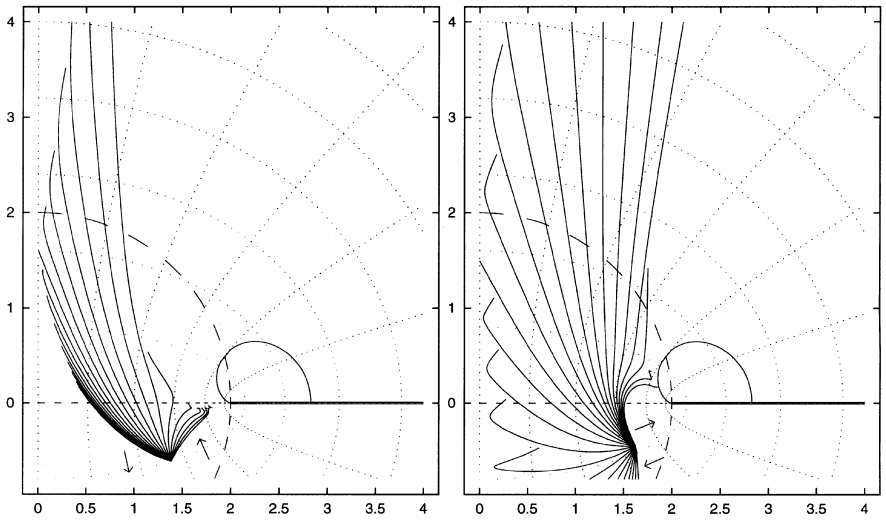

Figure 5. Particles released from rest ($\hat{\mathcal{V}}_{\rm in} = 0$) from $r < 0$ near the Kerr ring singularity with $a = 2M$. Left plot – $r_{\rm in} = -0.8M$, $\theta_{\rm in} = 40°$, initial spin pointing along/against local radial direction ($\hat{\alpha}^{\rm s}_{\rm in} = 0°/180°$): respectively from left to right (clockwise), 12 particles start with $\hat{\alpha}^{\rm s}_{\rm in} = 180°$ and $(\mathcal{M}\,M)^{-1}\,\hat{\mathcal{S}}_{\rm in} = 0.60, 0.55, 0.50, \ldots, 0.05$, the next one starts with zero spin (geodesic; it is the only trajectory that reaches the axis), and then 12 start with $\hat{\alpha}^{\rm s}_{\rm in} = 0°$ and $(\mathcal{M}\,M)^{-1}\,\hat{\mathcal{S}}_{\rm in} = 0.05, 0.10, 0.15, \ldots, 0.60$; the respective constants are $E/\mathcal{M} = 1.5175, 1.4984, 1.4794, 1.4604, 1.4414, 1.4223, 1.4033, 1.3843, 1.3652, 1.3462, 1.3272, 1.3082, 1.2891$ (geodesic), $1.2701, 1.2511, 1.2321, 1.2130, 1.1940, 1.1750, 1.1559, 1.1369, 1.1179, 1.0989, 1.0798, 1.0608$, and $(\mathcal{M}\,M)^{-1}\Phi = -0.3266, -0.2994, -0.2722, -0.2450, -0.2177, -0.1905, -0.1633, -0.1361, -0.1089, -0.0817, -0.0544, -0.0272, 0.0000$ (geodesic), $0.0272, 0.0544, \ldots, 0.3266$ (the third–sixth trajectories from the right display strange turns; the last five are stopped eventually where their tangents become space−like). Right plot – $r_{\rm in} = -0.7M$, $\theta_{\rm in} = 50°$, initial spin pointing along/against local latitudinal direction ($\hat{\alpha}^{\rm s}_{\rm in} = 90°$ and $\hat{\beta}^{\rm s}_{\rm in} = 0°/180°$): respectively from bottom to right (clockwise), 12 particles start with $\hat{\beta}^{\rm s}_{\rm in} = 180°$ and $(\mathcal{M}\,M)^{-1}\,\hat{\mathcal{S}}_{\rm in} = 0.60, 0.55, 0.50, \ldots, 0.05$, the next one starts with zero spin (geodesic; it reaches the axis), and then 12 start with $\hat{\beta}^{\rm s}_{\rm in} = 0°$ and $(\mathcal{M}\,M)^{-1}\,\hat{\mathcal{S}}_{\rm in} = 0.05, 0.10, 0.15, \ldots, 0.60$; the respective constants are $E/\mathcal{M} = 1.6360, 1.6173, 1.5986, 1.5799, 1.5612, 1.5425, 1.5237, 1.5050, 1.4863, 1.4676, 1.4489, 1.4302, 1.4115$ (geodesic), $1.3928, 1.3741, 1.3554, 1.3367, 1.3180, 1.2993, 1.2806, 1.2618, 1.2431, 1.2244, 1.2057, 1.1870$, and $(\mathcal{M}\,M)^{-1}\Phi = -0.0468, -0.0429, -0.0390, -0.0351, -0.0312, -0.0273, -0.0234, -0.0195, -0.0156, -0.0117, -0.0078, -0.0039, 0.0000$ (geodesic), $0.0039, 0.0078, \ldots, 0.0468$ (some of the last trajectories again display strange turns; the last two are stopped where their u^{μ} become space-like).

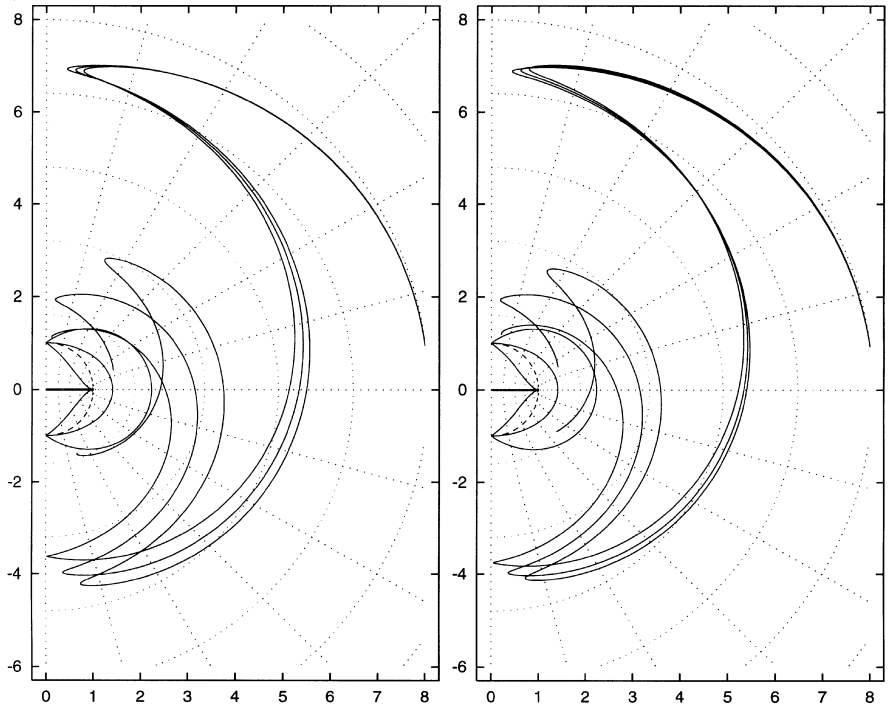

Figure 6. Late stages of inspiral of particles on to an extreme Kerr black hole ($a = M$): particles ejected tangentially ($\hat{\alpha}^{\rm v}_{\rm in} = 90°$, $\hat{\beta}^{\rm v}_{\rm in} = 175°$) from $r_{\rm in} = 8M$, $\theta_{\rm in} = 90°$ fall towards the hole along an almost polar orbit and hit the horizon at different points in dependence on their initial spin $\hat{\mathcal{S}}^{\mu}_{\rm in}$. The particle with $\hat{\mathcal{S}}_{\rm in} = 0.5\mathcal{M}\,M$ pointing downwards ($\hat{\alpha}^{\rm s}_{\rm in} = 90°$ $\hat{\beta}^{\rm s}_{\rm in} = 0°$) ends at the top pole, the one having $\hat{\mathcal{S}}_{\rm in} = 0$ (geodesic) ends in the equatorial region, whereas that with $\hat{\mathcal{S}}_{\rm in} = 0.5\mathcal{M}\,M$ pointing upwards ($\hat{\alpha}^{\rm s}_{\rm in} = 90°$ $\hat{\beta}^{\rm s}_{\rm in} = 180°$) reaches the bottom pole. In the left plot, all three particles have $E = 0.93385\mathcal{M}$, the corresponding initial speeds being respectively $\hat{\mathcal{V}}_{\rm in} = 0.368620$, 0.370000, 0.371365, and the angular momenta $(\mathcal{M}\,M)^{-1}\Phi = -0.1547$, 0.2804, 0.7154. In the right plot, all particles start with $\hat{\mathcal{V}}_{\rm in} = 0.37$, the corresponding energies being respectively $E/\mathcal{M} = 0.9344$, 0.9339, 0.9333, and the angular momenta $(\mathcal{M}\,M)^{-1}\Phi = -0.1534$, 0.2804, 0.7142. Integration was halted where the trajectories became space-like.

significant secular effect on the trajectory, namely can add or subtract a part of the orbit, perhaps a complete extra loop (or even several of them). This would bring an extra cycle (or cycles) of the gravitational wave.

It is important to compare Fig. 6 with Fig. 7 where similar trajectories were computed in a non-rotating, Schwarzschild background. In this case, nearly no divergence between trajectories occurs. Hence, one can attribute a substantial part of the spin-curvature effect to the spin–spin interaction (cf. again Figs 1 and 2, the Schwarzschild counterparts of which would only contain strictly radial paths).

5 CONCLUDING REMARKS

The figures prove that the spin-curvature interaction may lead to considerable deviations from geodesic motion. One should ask, however, whether the values of spin that already imply distinct effects may actually occur in nature, and whether they are compatible with the pole–dipole test-particle approximation. It seems that the answer is rather negative here. For an electron, for example, the specific spin $\tilde{S}$ is $(\hbar/2)/m_{\rm e} = 1.93\times10^{-11}$ cm. Hence, when expressed in units of mass of a compact stellar-size centre, with $M = 3\,{\rm M}_\odot = 4.43\times10^{5}$ cm, say, we obtain $S = 0.44\times10^{-16}m_{\rm e}M$. More promising than elementary particles appear to be whole stars orbiting around supermassive black holes in the nuclei of galaxies. Their specific angular momentum is considered to range from $10^{5}m_{\rm star}$ for a protostar of solar mass to $\leqslant m_{\rm star}$ for a neutron star (see de Felice & Sigalotti 1992). Then, for the most optimistic value and for the central mass $M = 10^{8}\,{\rm M}_\odot$, we arrive at $S \sim 10^{-3}m_{\rm star}M$. This is *not* negligible, but it is still no more than a lower limit at which *some* spin effect may be expected. Although a normal star therefore seems better than a pulsar, it is much harder to maintain the approximation for such a large and easily deformable body. For a stellar-size compact object (a pulsar or a black hole), with mass $m_{\rm comp} \sim {\rm M}_\odot$ and specific spin approaching its extreme value $m_{\rm comp}$, the pole–dipole test-particle approximation could probably hold for not fairly close orbits around a Kerr black hole of mass down to the value $M \sim 10^{3}\,{\rm M}_\odot$. For such a (rather hypothetical) situation, one again reaches only $S \sim 10^{-3}m_{\rm comp}M$, which can only result in *secular* deviations from a freely falling trajectory. Even these may be important, however, e.g. in gradual spiralling of a pulsar towards a massive Kerr hole, which should be resolvable in gravitational waves some day. Very large spin effects can then be expected in situations where one deals not with motion of a spinning 'particle' in the field of a much more massive body, but with a two-particle problem with spins, e.g. in binary pulsars (see Apostolatos 1996).

With large spins, u^{μ} easily becomes space-like close to the source. We halted the integration of a trajectory when such a point was reached (it is indicated in the figure captions). If one does not care about this indication of the limits of applicability of the MP equations, very illogical motions may be obtained with sudden changes of direction, etc. It is a question, however, as to whether this indication is reliable (i.e. necessary and sufficient). Some

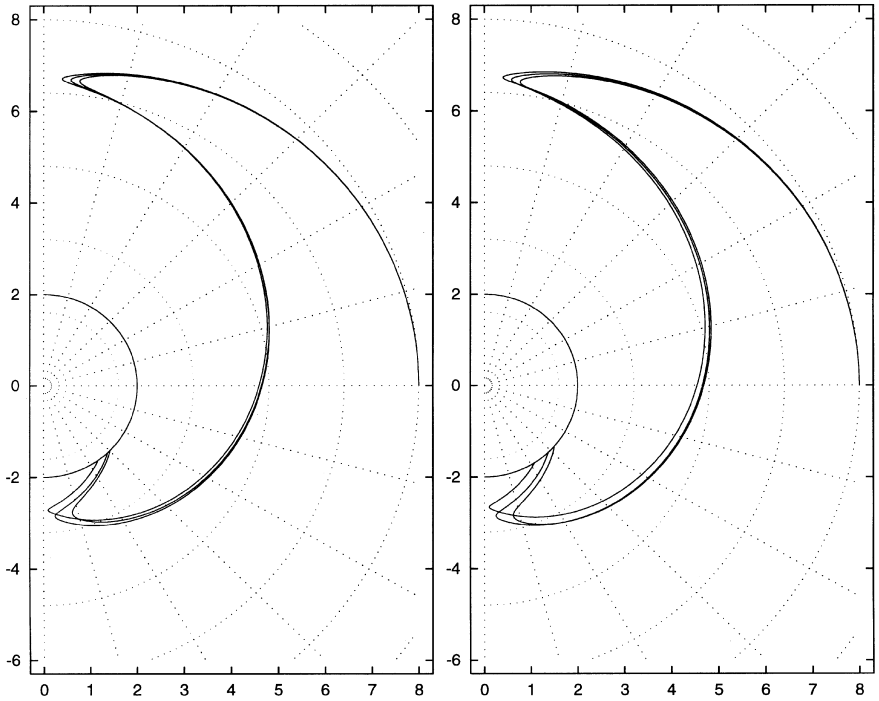

Figure 7. Schwarzschild ($a = 0$) counterpart of Fig. 6; the spin effect is much weaker than in the extreme Kerr case. In the left plot, all three particles have $E = 0.932182\mathcal{M}$, the corresponding initial speeds being respectively $\hat{\mathcal{V}}_{\rm in} = 0.370730$, 0.370000, 0.369272, and the angular momenta $(\mathcal{M}M)^{-1}\Phi = -0.1552$, 0.2777, 0.7106. In the right plot, all particles start with $\hat{\mathcal{V}}_{\rm in} = 0.37$, the corresponding energies being respectively $E/\mathcal{M} = 0.9319$, 0.9322, 0.9325, and the angular momenta $(\mathcal{M}M)^{-1}\Phi = -0.1558$, 0.2777, 0.7112.

paths already bend in a suspect way *near* the region where u^μ becomes space-like. This can mainly be noticed in the initial deflections of certain trajectories ejected from the vicinity of the source – see the initial parts of the trajectories in the left and right plots of Fig. 1. In such situations, u^μ usually differs from $\mathcal{U}^\mu$ considerably, so the particle may also start in quite a different direction (given by u^μ) from what one would expect according to the initial $\mathcal{U}^\mu$. Strange bends are also illustrated in Fig. 5, where particles that have been released from rest ($\mathcal{U}^\mu = 0$) from 'the other side of the singularity' ($r_{\rm in} = -0.8M, -0.7M$) with different spins are followed.

Hence, the question also arises of whether it would not be better to fix, instead of the initial $\mathcal{U}^\mu$, the initial u^μ, even if the integration logic requires, in the case of our choice of the spin supplementary condition (20), one to *calculate* the u^μ from $\mathcal{U}^\mu$ and $S^{\mu\nu}$ in each step. Should not one still adhere to the other supplementary condition, (19), as also suggested by Ragusa & Bailyn (1995), however? The relation between u^μ and p^μ (the counterpart of equation 34) is not known in this case, but we could perhaps use the u^μ from a preceding step in the integration. Although the integration step would not be 'closed' as nicely as in our case here, this might not bring serious inaccuracy if the step in proper time is chosen to be sufficiently small.

It was demonstrated by Barker & O'Connell (1974) that even when keeping only second-order terms in the spin or velocity of the particle or in the gravitational radius of the centre, the different supplementary conditions lead to different non-geodesic equations of motion. It would therefore be interesting to compare the trajectories obtained with different supplementary conditions. This is our aim for the second paper in this series.

ACKNOWLEDGMENTS

I thank Professor Jan Horský for suggesting the topic, Professor Jiří Bičák for Plyatsko's book, and my brother Ivan for assembling such a cheap PC. Professor B. Schutz suggested computing the polar inspiral, where a cumulative effect can be important. I acknowledge support from the grants GACR-202/99/0261 of the Grant Agency of the Czech Republic and GAUK-230/96 of the Charles University.

REFERENCES

Abramowicz M. A., Calvani M., 1979, MNRAS, 189, 621
Aguirregabiria J. M., Chamorro A., Suinaga J., Vishveshwara C. V., 1996, Class. Quantum Grav., 13, 417
Apostolatos T. A., 1996, Class. Quantum Grav., 13, 799
Apostolatos T. A., Cutler C., Sussman G. J., Thorne K. S., 1994, Phys. Rev. D, 49, 6274
Bailyn M., Ragusa S., 1977, Phys. Rev. D, 15, 3543
Bailyn M., Ragusa S., 1981, Phys. Rev. D, 23, 1258
Barker B. M., O'Connell R. F., 1974, Gen. Rel. Grav., 5, 539
Barker B. M., O'Connell R. F., 1979, Gen. Rel. Grav., 11, 149
Beiglböck W., 1967, Commun. Math. Phys., 5, 106
Bičák J., Semerák O., Hadrava P., 1993, MNRAS, 263, 545
Bonazzola S., 1964, Nuovo Cim., 33, 1584
Bretón N., Manko V. S., 1995, Class. Quantum Grav., 12, 1969
Caderni N., Calvani M., 1979, Phys. Lett. A, 71, 1
Calvani M., 1980, Nuovo Cimento A, 58, 364
Carmeli M., Charach Ch., Kaye M., 1977, Phys. Rev. D, 15, 1501
Chandrasekhar S., 1983, The Mathematical Theory of Black Holes, Clarendon Press, Oxford

Corinaldesi E., Papapetrou A., 1951, Proc. R. Soc. London, Ser. A, 209, 259
Damour T., 1987, in Hawking S. W., Israel W., eds, 300 Years of Gravitation. Cambridge Univ. Press, Cambridge, p. 128
Damour T., Soffel M., Xu Ch., 1991, Phys. Rev. D, 43, 3273
de Felice F., Sigalotti L., Di G., 1992, ApJ, 389, 386
Dietz W., Hoenselaers C., 1982, Phys. Rev. Lett., 48, 778
Dietz W., Hoenselaers C., 1985, Ann. Phys. (NY), 165, 319
Dixon W. G., 1964, Nuovo Cimento, 34, 317
Dixon W. G., 1970, Proc. R. Soc. London, Ser. A, 314, 499
Dixon W. G., 1979, in Ehlers J., ed., Proc. Int. School of Physics 'Enrico Fermi', Course LXVII, Isolated Gravitating Systems in General Relativity. North Holland, Amsterdam, p. 156
Duval C., Fliche H. H., 1978, J. Math. Phys., 19, 749
Dymnikova I. G., 1986, Sov. Phys. – Usp., 29, 215
Ehlers J., Rudolph E., 1977, Gen. Rel. Grav., 8, 197
Frenkel J., 1926, Z. Phys., 37, 243 (in German)
Fuchs H., 1983, Ann. Phys. (Leipzig), 40, 47
Hojman S., 1978, Phys. Rev. D, 18, 2741
Hojman R., Hojman S., 1977, Phys. Rev. D, 15, 2724
Infeld L., Schild A., 1949, Rev. Mod. Phys., 21, 408
Kidder L. E., 1995, Phys. Rev. D, 52, 821
Krivenko O. P., Pyragas K. A., Zhuk I. T., 1976, Ap&SS, 40, 39
Künzle H. P., 1972, J. Math. Phys., 13, 739
Lanczos C., 1929, Z. Phys., 59, 514 (in German)
Leterier P. S., de Oliveira S. R., 1998, Phys. Lett. A, 238, 101
Madore J., 1969, Ann. Inst. Henri Poincaré A, 11, 221
Manko V. S., Martín J., Ruiz E., 1994, J. Math. Phys., 35, 6644
Mashhoon B., 1971, J. Math. Phys., 12, 1075
Mashhoon B., 1975, Ann. Phys. (NY), 89, 254
Mathisson M., 1937, Acta Phys. Polon., 6, 163 (in German)
Mathisson M., 1940, Proc. Camb. Phil. Soc., 36, 331
Micoulaut R., 1967, Z. Phys., 206, 394 (in German)
Mino Y., Shibata M., Tanaka T., 1996, Phys. Rev. D, 53, 622
Misner C. W., Thorne K. S., Wheeler J. A., 1973, Gravitation. Freeman, San Francisco
Møller C., 1949, Commun. Dublin Inst. Adv. Studies A, 5, 3
Nevin J. M., 1995, Gen. Rel. Grav., 27, 397
O'Connell R. F., 1974, in Bertotti B., ed., Proc. Int. School of Physics 'Enrico Fermi', Course LVI, Experimental Gravitation. Academic Press, New York, p. 496
Omote M., 1973, Prog. Theor. Phys., 49, 1559
Papapetrou A., 1951, Proc. R. Soc. London, Ser. A, 209, 248
Papapetrou A., Urich W., 1955, Z. Naturforsch., A, 10, 109 (in German)
Pfister H., Schedel Ch., 1987, Class. Quantum Grav., 4, 141
Pirani F. A. E., 1956, Acta Phys. Polon., 15, 389
Plyatsko R. M., 1988, The manifestations of the ultra-relativistic spin-orbital interaction. Naukova Dumka, Kiev (in Ukrainian)
Prasanna A. R., Kumar N., 1973, Prog. Theor. Phys., 49, 1553
Prasanna A. R., Virbhadra K. S., 1989, Phys. Lett. A, 138, 242
Pryce M. H. L., 1948, Proc. R. Soc. London, Ser. A, 195, 62
Ragusa S., Bailyn M., 1995, Gen. Rel. Grav., 27, 163
Rasband S. N., 1973, Phys. Rev. Lett., 30, 111
Ray J. R., Smalley L. L., 1982, Phys. Rev. D, 26, 2619
Rees M. J., 1998, in Wald R. M., ed., Black Holes and Relativistic Stars. Univ. Chicago Press, Chicago, p. 79
Rüdiger R., 1981, Proc. R. Soc. London, Ser. A, 375, 185
Rüdiger R., 1983, Proc. R. Soc. London, Ser. A, 385, 229
Schattner R., 1979a, Gen. Rel. Grav., 10, 377
Schattner R., 1979b, Gen. Rel. Grav., 10, 395
Schiff L. I., 1960, Proc. Natl. Acad. Sci., 46, 871
Semerák O., 1996, Class. Quantum Grav., 13, 2987
Semerák O., 1997, Gen. Rel. Grav., 29, 153
Semerák O., 1999, in Ruffini R., Sigismondi C., eds, Proc. Third W. Fairbank Meeting, The Lense–Thirring Effect. World Sci., Singapore, in press
Sharp N. A., 1979, Gen. Rel. Grav., 10, 659
Stewart J., Walker M., 1973, Springer Tracts Mod. Phys., 69, 69
Suzuki S., Maeda K., 1997, Phys. Rev. D, 55, 4848
Synge J. L., 1935, Phys. Rev., 47, 760
Tafel J., 1980, Gen. Rel. Grav., 12, 1035
Tanaka T., Mino Y., Sasaki M., Shibata M., 1996, Phys. Rev. D, 54, 3762
Taub A. H., 1964, J. Math. Phys., 5, 112
Thorne K. S., Hartle J. B., 1985, Phys. Rev. D, 31, 1815
Tod K. P., de Felice F., Calvani M., 1976, Nuovo Cimento B, 34, 365
Tulczyjew W., 1959, Acta Phys. Polon., 18, 393
Wald R., 1972, Phys. Rev. D, 6, 406
Wald R., 1974, Ann. Phys. (NY), 83, 548
Weyssenhoff J., 1947a, Acta Phys. Polon., 9, 26
Weyssenhoff J., 1947b, Acta Phys. Polon., 9, 34
Weyssenhoff J., Raabe A., 1947a, Acta Phys. Polon., 9, 7
Weyssenhoff J., Raabe A., 1947b, Acta Phys. Polon., 9, 19
Wilkins D. C., 1970, Ann. Phys. (NY), 61, 277

APPENDIX A: CHRISTOFFEL SYMBOLS AND RIEMANN TENSOR OF THE KERR METRIC

There are 32 non-zero Christoffel symbols of the Kerr metric, 24 of which are equal in pairs. In Boyer–Lindquist coordinates they are given by the following relations:

$$\frac{\Gamma^t_{tr}}{r^2+a^2}=\frac{\Gamma^\phi_{tr}}{a}=\frac{M}{\Delta\Sigma^2}(2r^2-\Sigma),$$

$$\frac{\Gamma^t_{t\theta}}{a\sin^2\theta}=\Gamma^\phi_{t\theta}=-\frac{2Mar}{\Sigma^2}\cot\theta,$$

$$\Delta\Sigma^2\Gamma^t_{r\phi}=-Ma[2r^2(r^2+a^2)+\Sigma(r^2-a^2)]\sin^2\theta,$$

$$\Delta\Sigma^2\Gamma^\phi_{r\phi}=r\Sigma(\Sigma-2Mr)-Ma^2(2r^2-\Sigma)\sin^2\theta,$$

$$\Sigma^2\Gamma^t_{\theta\phi}=Ma^3r\sin^2\theta\sin2\theta,$$

$$\Sigma^2\Gamma^\phi_{\theta\phi}=(\mathcal{A}-\Sigma a^2\sin^2\theta)\cot\theta,$$

$$\Gamma^r_{tt}=-\frac{\Gamma^r_{t\phi}}{a\sin^2\theta}=\frac{M\Delta}{\Sigma^3}(2r^2-\Sigma),$$

$$-\frac{\Gamma^\theta_{tt}}{a}=\frac{\Gamma^\theta_{t\phi}}{r^2+a^2}=\frac{Mar}{\Sigma^3}\sin2\theta,$$

$$\Gamma^r_{rr}=\frac{r}{\Sigma}+\frac{M-r}{\Delta},\qquad -\Gamma^r_{\theta\theta}=\Delta\Gamma^\theta_{r\theta}=\frac{r\Delta}{\Sigma},$$

$$\Gamma^r_{r\theta}=\Gamma^\theta_{\theta\theta}=-\Delta\Gamma^\theta_{rr}=-\frac{a^2\sin2\theta}{2\Sigma},$$

$$\Sigma^3\Gamma^r_{\phi\phi}=-\Delta[r\Sigma^2-Ma^2(2r^2-\Sigma)\sin^2\theta]\sin^2\theta,$$

$$2\Sigma^3\Gamma^\theta_{\phi\phi}=-[\Delta\Sigma^2+2Mr(r^2+a^2)^2]\sin2\theta.$$

For quick reference, we give all the (non-zero) Boyer–Lindquist components of the Riemann tensor, with the only exception being those that follow immediately by just commuting the last two indices. All the non-zero components contain the factor M. Other major regularities present in the list below are bound up with how many indices occur from the set (r,θ): (i) the total number of indices of this type must be even (0, 2 or 4); (ii) components with an even number (0 or 2) of one (or each) of these two indices contain the factor $X=r^2-3a^2\cos^2\theta$, whereas those with an odd number of each of these indices (namely with one index r and one index θ) contain the factor $Y=3r^2-a^2\cos^2\theta$.

$$R^t_{tt\phi} = -R^\phi_{\phi t\phi} = -\omega_{\rm K} R^t_{\phi t\phi} = -\frac{2Mar}{\Delta - a^2\sin^2\theta} R^\phi_{tt\phi}$$
$$= \frac{2M^2ar^2}{\Sigma^4} X\sin^2\theta,$$
$$R^t_{tr\theta} = -R^\phi_{\phi r\theta} = -\omega_{\rm K} R^t_{\phi r\theta} = -\frac{2Mar}{\Delta - a^2\sin^2\theta} R^\phi_{tr\theta}$$
$$= -\frac{M^2a^2r}{\Delta\Sigma^3} Y\sin 2\theta,$$
$$\Delta R^t_{rtr} = -R^\phi_{\theta\theta\phi} = Mr\Sigma^{-3}X[2(r^2+a^2) + a^2\sin^2\theta],$$
$$-R^t_{\theta t\theta} = \Delta R^\phi_{rr\phi} = Mr\Sigma^{-3}X(r^2 + a^2 + 2a^2\sin^2\theta),$$
$$R^t_{rt\theta} = R^\phi_{r\theta\phi} = -Ma^2\Delta^{-1}\Sigma^{-3}Y[3(r^2+a^2) - 2Mr]\sin\theta\cos\theta,$$
$$R^t_{\theta tr} = R^\phi_{\theta r\phi} = -Ma^2\Delta^{-1}\Sigma^{-3}Y[3(r^2+a^2) - 4Mr]\sin\theta\cos\theta,$$
$$\Delta R^t_{rr\phi} = -R^t_{\theta\theta\phi} = 3Mar\Sigma^{-3}(r^2+a^2)X\sin^2\theta,$$
$$\Delta R^\phi_{rtr} = -R^\phi_{\theta t\theta} = 3Mar\Sigma^{-3}X,$$
$$R^r_{tt\theta} = \Delta R^\theta_{ttr} = -3Ma^2\Delta\Sigma^{-4}Y\sin\theta\cos\theta,$$
$$R^r_{tr\phi} = -R^r_{\phi tr} = Mar\Sigma^{-4}X[3(r^2+a^2) - 4Mr]\sin^2\theta,$$
$$-R^\theta_{t\theta\phi} = R^\theta_{\phi t\theta} = Mar\Sigma^{-4}X[3(r^2+a^2) - 2Mr]\sin^2\theta,$$
$$-R^r_{t\theta\phi} = \Delta R^\theta_{\phi tr} = Ma\Delta\Sigma^{-4}Y[2(r^2+a^2) + a^2\sin^2\theta]\sin\theta\cos\theta,$$
$$R^r_{\phi t\theta} = -\Delta R^\theta_{tr\phi} = Ma\Delta\Sigma^{-4}Y(r^2 + a^2 + 2a^2\sin^2\theta)\sin\theta\cos\theta,$$
$$R^r_{\theta t\phi} = -\Delta R^\theta_{rt\phi} = \frac{\Delta^2}{2Mar} R^t_{tr\theta},$$
$$R^r_{\phi\theta\phi} = \Delta R^\theta_{\phi r\phi} = -(r^2+a^2)R^r_{tt\theta}\sin^2\theta,$$
$$-R^r_{\theta r\theta} = \Delta R^\theta_{rr\theta} = Mr\Sigma^{-2}X,$$
$$\Delta\Sigma^3 R^t_{r\theta\phi} = -MaY[2(r^2+a^2)^2 + \Delta a^2\sin^2\theta]\sin\theta\cos\theta,$$
$$\Delta\Sigma^3 R^t_{\theta r\phi} = -MaY[(r^2+a^2)^2 + 2\Delta a^2\sin^2\theta]\sin\theta\cos\theta,$$
$$\Delta\Sigma^3 R^\phi_{rt\theta} = -MaY(\Delta + 2a^2\sin^2\theta)\cot\theta,$$
$$\Delta\Sigma^3 R^\phi_{\theta tr} = -MaY(2\Delta + a^2\sin^2\theta)\cot\theta,$$
$$\Sigma^4 R^r_{ttr} = MrX(2\Delta + a^2\sin^2\theta),$$
$$\Sigma^4 R^\theta_{tt\theta} = -MrX(\Delta + 2a^2\sin^2\theta),$$
$$\Sigma^4 R^r_{\phi r\phi} = -MrX[(r^2+a^2)^2 + 2\Delta a^2\sin^2\theta]\sin^2\theta,$$
$$\Sigma^4 R^\theta_{\phi\theta\phi} = MrX[2(r^2+a^2)^2 + \Delta a^2\sin^2\theta]\sin^2\theta.$$

This paper has been typeset from a TEX/LATEX file prepared by the author.